SIAM J. SCI. COMPUT.
Vol. 34, No. 3, pp. A1607–A1634

CHOOSING THE BEST KERNEL: PERFORMANCE MODELS FOR DIFFUSION OPERATORS IN PARTICLE METHODS*

BIRTE SCHRADER†, SYLVAIN REBOUX†, AND IVO F. SBALZARINI†

Abstract. In scientific simulations of partial differential equations one is often faced with the task of choosing a discretization scheme or tuning the parameters of a discretized differential operator to perform well on a given problem. While this is mostly done through benchmark simulations on test problems, a problem-independent performance model would be desirable. Based on results from numerical analysis, we present a set of problem-independent performance measures for diffusion operators in particle methods. These measures quantify an operator's accuracy, stability, and computational cost. They can be explicitly derived in closed form, hence enabling comparisons between different operators and operator parameter tuning without the need for running any benchmark simulations. If a small number of benchmarks is available, a regression over the quality measures can be calibrated to absolute CPU time, hence defining predictive performance models for the different operators. We demonstrate this on the example of PSE operators and show the computational savings that can be achieved by operator selection and tuning.

Key words. particle method, diffusion operator, performance model, kernel choice, operator parameters, particle strength exchange (PSE), discretization-corrected PSE

AMS subject classifications. 15A15, 15A09, 15A23

DOI. 10.1137/110835815

1. Introduction.

Numerical methods for partial differential equations are usually designed with aims such as accuracy, robustness, computational efficiency, and ease of implementation. These objectives are often conflicting, implying trade-offs in the method design. As a consequence, an abundance of numerical methods has been designed to discretize the same differential operator, each method having its characteristic design emphasis and qualities. In this wealth of choices it is not always easy to select the most efficient method to solve a given problem in computational science and engineering to a desired level of accuracy. Method choice and performance quantification are most often based on results obtained on model problems or benchmark test cases. For some linear operators, like diffusion operators, however, a priori error estimates can be obtained that provide valuable information about the a posteriori errors in a particular application. This is in contrast to nonlinear or integral operators, where error estimates and stability conditions can be prohibitively complicated or even unavailable, and a priori performance quantification is usually beyond reach.

If problem-independent a priori performance estimates are available, the number of benchmark tests that need to be conducted in order to select a method or tune its parameters can be reduced, and transferability of results between different applications improved. Such a problem-independent performance model could then be matched, on the one hand, to the needs of an application, and on the other hand

*Submitted to the journal's Methods and Algorithms for Scientific Computing section May 31, 2011; accepted for publication (in revised form) March 14, 2012; published electronically June 19, 2012. This work was supported by the Swiss National Science Foundation (SNSF) through grants 200021-132064 and 200021-115764 and by the Swiss SystemsX.ch initiative through grant LipidX-2008/011, evaluated by the Swiss National Science Foundation.

http://www.siam.org/journals/sisc/34-3/83581.html

†MOSAIC Group, Institute of Theoretical Computer Science and Swiss Institute of Bioinformatics, ETH Zürich, Universitätstr. 6, CH-8092 Zürich, Switzerland (birte@ethz.ch, sylvain.reboux@inf.ethz.ch, ivos@ethz.ch).

to the resource offerings of specific hardware architectures. The former can, e.g., be done by statistical regression, the latter through hardware performance models such as rooflines [34] or the κ–Γ model [16].

Here, we provide a set of problem-independent performance measures for isotropic and anisotropic diffusion operators in particle methods. Approximation of the elliptic diffusion operator $L(\cdot) = \nabla \cdot (\boldsymbol{\nu} \nabla(\cdot))$, $\boldsymbol{\nu} > 0$, is commonly required in numerical simulations from fluid dynamics to electromagnetism and quantum physics. Particle methods provide mesh-free discretization schemes that are particularly advantageous for convection-dominated problems or problems in complex geometries [18]. A variety of methods for treating the diffusion operator in particle methods exists. This includes the methods of random walk [3] and of deterministic displacements [11]. More accurate methods include resampling methods [7, 27], redistribution methods [28, 29, 32, 15], particle strength exchange (PSE) methods [22, 9, 10, 13, 12, 31], smoothed particle hydrodynamics (SPH) [25], moving least squares [19, 1, 14], and reproducing kernel particle methods [21, 20]. Each of these approaches has its characteristic properties and, in addition, many operators have free parameters with which their properties can be further tuned [26, 2, 12]. This raises the question of how to choose an operator for a given problem at hand, how to best set its parameters, and how much one can potentially gain by doing so.

We address this question by introducing three problem-independent measures to quantify the accuracy, computational cost, and stability of diffusion operators in particle methods. The "operator quality measures" presented here are problem-independent in the sense that they are only functions of the operator type and parameters, but not of the field functions the operator is later going to be applied on. Problem-independent operator characteristics are well known, e.g., in the form of convergence orders. However, while the convergence order tells how the numerical approximation error is expected to decrease with increasing resolution of the method, it does not provide any information about the magnitude of the error that can be expected at a certain resolution, or about the runtime of the simulation. The operator quality measures presented here constitute features in a machine-learning sense, i.e., characteristic properties that are designed to have predictive power. Since they can be explicitly derived from numerical analysis, they allow testing and comparison of large numbers of operators or parameter settings without performing benchmark simulations. We derive closed-form expressions of the measures introduced here for PSE and Fishelov diffusion operators, and for the diffusion operators used in a resampling method and in SPH. This enables parameter studies and visualization of the parameter spaces of operators in "phase diagrams" akin to those used in physics and chemistry.

In order to predict the expected performance of a given operator on a certain problem, a small number of benchmark simulations of that problem is used to calibrate the quality measures to actual CPU time, hence identifying an a posteriori runtime model from the benchmark data. These calibration curves are valid for all operator parameters, but only for the specific problem (implementation, compiler, hardware) they have been measured on. They thus directly account for the influences of the implementation, hardware, etc., on the simulation runtime. The operator minimizing the predicted CPU time under certain constraints can then be selected purely based on its quality measures, without running any further benchmarks. This enables automatic choice of the most efficient operator in a simulation code. We show that these *appointed* operators outperform other standard operator choices for a

three-dimensional advection-diffusion problem. In the case study presented here, the computational savings are at least a factor of two compared to the next-best tested operator.

The paper is organized as follows: In the next section, we briefly recall the general form of diffusion operators in particle methods. Section 3 introduces the concept of problem-independent operator quality measures and shows their derivation for the example of isotropic PSE diffusion operators. Then, in section 4, we generalize to three quality measures, for which closed-form expressions for four different types of diffusion operators are given in Appendix A. We analyze the dependence of operator qualities on parameter choices in section 5 using PSE operators as an example, providing parameter landscapes for this class of operators. In section 6, we demonstrate how the presented quality measures can be calibrated to construct a predictive performance model for different operators in a real-world application. We further quantify the computational savings that can be achieved by choosing and tuning the operator for the problem at hand. We conclude this work and discuss some of the implications and possible follow-ups in section 7.

2. Diffusion operators in particle methods. Diffusion operators $Q^h(\cdot)$ in particle methods approximate the operator $L(\cdot)$ defined by

$$Lf(\boldsymbol{x}) = \nabla \cdot (\boldsymbol{\nu}(\boldsymbol{x}) \nabla f(\boldsymbol{x})) = \sum_{i,j=1}^{n} D^{\boldsymbol{e}_i} \left[\nu_{ij}(\boldsymbol{x}) D^{\boldsymbol{e}_j} f(\boldsymbol{x}) \right] , \tag{2.1}$$

where f is any twice differentiable function over $\mathbb{R}^n$, ν_{ij} are the elements of the symmetric positive definite diffusion tensor $\boldsymbol{\nu} \in \mathbb{R}^{n \times n}$, and $\boldsymbol{e}_i$ is the unit vector along dimension i. In the case of isotropic diffusion, ν is a scalar viscosity and the operator simplifies to

$$Lf(\boldsymbol{x}) = \nabla \cdot (\nu(\boldsymbol{x}) \nabla f(\boldsymbol{x})) = \sum_{|\boldsymbol{\alpha}|=1} \left[D^{\boldsymbol{\alpha}} \nu(\boldsymbol{x}) D^{\boldsymbol{\alpha}} f(\boldsymbol{x}) + \nu(\boldsymbol{x}) D^{2\boldsymbol{\alpha}} f(\boldsymbol{x}) \right] . \tag{2.2}$$

These operators are discretized over a set of particles that sample the field $f(\boldsymbol{x})$ and the viscosity $\nu(\boldsymbol{x})$ at locations $\boldsymbol{x}_p$, $p = 1, \ldots, N$, hence $f_p = f(\boldsymbol{x}_p)$ and $\nu_p = \nu(\boldsymbol{x}_p)$. Here, $\boldsymbol{\alpha} = (\alpha_1, \ldots, \alpha_n) \in \mathbb{N}^n$ is a multi-index, and n is the number of space dimensions. Multi-index notation,

$$|\boldsymbol{\alpha}| = \sum_{i=1}^{n} \alpha_i, \quad \boldsymbol{x}^{\boldsymbol{\alpha}} = x_1^{\alpha_1} x_2^{\alpha_2} \ldots x_n^{\alpha_n}, \quad D^{\boldsymbol{\alpha}} f(\boldsymbol{x}) = \frac{\partial^{|\boldsymbol{\alpha}|} f(\boldsymbol{x})}{\partial x_1^{\alpha_1} \partial x_2^{\alpha_2} \ldots \partial x_n^{\alpha_n}},$$

is used throughout this work. The notation $\sum_{|\boldsymbol{\alpha}|=a}^{b}$ denotes a sum over all multi-indices $\boldsymbol{\alpha}$ for which $a \leq |\boldsymbol{\alpha}| \leq b$ and $\sum_{|\boldsymbol{\alpha}|=a}$ is equivalent to $\sum_{|\boldsymbol{\alpha}|=a}^{a}$.

The Sobolev norms $W^{m,\infty}(\Omega)$ are defined as

$$\|u\|_{W^{m,\infty}(\Omega)} = \max_{0 \leq |\boldsymbol{\alpha}| \leq m} \|D^{\boldsymbol{\alpha}} u\|_{L^\infty(\Omega)}.$$

In smooth particle methods, continuous quantities are discretized onto a set of particles with positions $\boldsymbol{x}_p$ and volumes v_p using smoothing kernels of width ε. The characteristic distance between particles is denoted by h. We define the ratio $c = h/\varepsilon$. The operators in (2.1)–(2.2) are typically expressed as sums running over the particles located in an r_c-neighborhood of $\boldsymbol{x}$, where the parameter r_c is called the cutoff radius.

The accuracy and the stability of the discretized operators depend on the choice of the kernel function, the cutoff radius, and the ratio c. Many choices are legitimate, in the sense that they yield a convergent approximation, but they are not all equally pertinent as they may lead to different errors, stability conditions, and computational costs. These quantities can be analyzed a priori, thus providing a performance model to rationalize the choice of operator parameters.

3. Assessing the quality of PSE diffusion operators. Particle strength exchange (PSE) diffusion operators were introduced by Degond and Mas-Gallic for the cases of isotropic [9] and anisotropic [10] viscosity. Their discretization-corrected (DC) versions have been discussed by Schrader, Reboux, and Sbalzarini [31].

As a motivating example for the rest of the paper, we briefly restate PSE diffusion operators with isotropic viscosity and show how their accuracy and stability can be characterized a priori from an error analysis. Examples of analogous derivations for other discrete operators can be found in Appendix A.

The PSE operator approximating the operator $L(\cdot)$ from (2.2) is defined as

$$Q_h f(\boldsymbol{x}) = \frac{c^n}{\varepsilon^2} \sum_{p \in \mathcal{N}(\boldsymbol{x})} \frac{v_p}{h^n} \left(f(\boldsymbol{x}_p) - f(\boldsymbol{x})\right) \mu(\boldsymbol{x}, \boldsymbol{x}_p) \eta\left(\frac{\boldsymbol{x} - \boldsymbol{x}_p}{\varepsilon}\right), \tag{3.1}$$

where $\mathcal{N}(\boldsymbol{x})$ is the index set of the particles contained in the closed ball $B_{r_c}[\boldsymbol{x}] = \{\boldsymbol{y} \in \mathbb{R}^n : |\boldsymbol{y} - \boldsymbol{x}| \leq r_c\}$. The cutoff radius r_c is typically chosen such that this r_c-neighborhood coincides (with a certain accuracy) with the support of the kernel function η. For conservation of mass when using identical operators $Q_h(\cdot)$ on all particles, $\mu(\boldsymbol{x}, \boldsymbol{y})$ is chosen to be the symmetric mean of $\nu(\boldsymbol{x})$ and $\nu(\boldsymbol{y})$.

For any particle $\boldsymbol{x}_p$, a Taylor expansion of f and ν around $\boldsymbol{x}$ yields

$$\begin{aligned} &\mu(\boldsymbol{x}, \boldsymbol{x}_p)(f(\boldsymbol{x}_p) - f(\boldsymbol{x})) \\ &\quad = \sum_{|\boldsymbol{\alpha}|=1}^{r+1} \frac{D^{\boldsymbol{\alpha}} f(\boldsymbol{x})}{\boldsymbol{\alpha}!} \left[\nu(\boldsymbol{x})(\boldsymbol{x}_p - \boldsymbol{x})^{\boldsymbol{\alpha}} + \sum_{|\boldsymbol{\beta}|=1}^{r+1} \frac{D^{\boldsymbol{\beta}} \nu(\boldsymbol{x})}{2\boldsymbol{\beta}!} (\boldsymbol{x}_p - \boldsymbol{x})^{\boldsymbol{\alpha}+\boldsymbol{\beta}}\right] \\ &\quad + \sum_{|\boldsymbol{\alpha}|=r+2} R_{\boldsymbol{\alpha}}(\boldsymbol{x}_p) \mu(\boldsymbol{x}, \boldsymbol{x}_p)(\boldsymbol{x}_p - \boldsymbol{x})^{\boldsymbol{\alpha}}, \end{aligned} \tag{3.2}$$

where the remainder $R_{\boldsymbol{\alpha}}(\boldsymbol{y})$ is bounded by

$$|R_{\boldsymbol{\alpha}}(\boldsymbol{y})| \leq \frac{|\boldsymbol{\alpha}|}{\boldsymbol{\alpha}!} \max_{|\boldsymbol{\beta}|=|\boldsymbol{\alpha}|} \max_{\boldsymbol{z} \in B_{r_c}[\boldsymbol{x}]} |D^{\boldsymbol{\beta}} f(\boldsymbol{z})|. \tag{3.3}$$

Multiplying (3.2) by $v_p \eta((\boldsymbol{x}_p - \boldsymbol{x})/\varepsilon)/\varepsilon^n$ and summing over the particles in $\mathcal{N}(\boldsymbol{x})$ leads to

$$\begin{aligned} Q_h f(\boldsymbol{x}) = &\sum_{|\boldsymbol{\alpha}|=1}^{r+1} \frac{D^{\boldsymbol{\alpha}} f(\boldsymbol{x})}{\boldsymbol{\alpha}!} \left[h^{|\boldsymbol{\alpha}|-2} \nu(\boldsymbol{x}) Z_h^{\boldsymbol{\alpha}} + \sum_{|\boldsymbol{\beta}|=1}^{r+1} h^{|\boldsymbol{\alpha}+\boldsymbol{\beta}|-2} \frac{D^{\boldsymbol{\beta}} \nu(\boldsymbol{x})}{2\boldsymbol{\beta}!} Z_h^{\boldsymbol{\alpha}+\boldsymbol{\beta}}\right] \\ &+ h^r c^n \sum_{|\boldsymbol{\alpha}|=r+2} \sum_{p \in \mathcal{N}(\boldsymbol{x})} \frac{v_p}{h^n} R_{\boldsymbol{\alpha}}(\boldsymbol{x}_p) \eta\left(c \frac{\boldsymbol{x}_p - \boldsymbol{x}}{h}\right) \mu(\boldsymbol{x}, \boldsymbol{x}_p) \left(\frac{\boldsymbol{x}_p - \boldsymbol{x}}{h}\right)^{\boldsymbol{\alpha}}, \end{aligned} \tag{3.4}$$

where the discrete moments of η, $Z_h^{\boldsymbol{\alpha}}$, are defined as

$$Z_h^{\boldsymbol{\alpha}}(\boldsymbol{x}) = c^{n+2} \sum_{p \in \mathcal{N}(\boldsymbol{x})} \frac{v_p}{h^n} \left(\frac{\boldsymbol{x} - \boldsymbol{x}_p}{h} \right)^{\boldsymbol{\alpha}} \eta \left(c \frac{\boldsymbol{x} - \boldsymbol{x}_p}{h} \right). \tag{3.5}$$

Defining the functions $A_s(\boldsymbol{x}) \in \mathbb{R}^+ \cup \{\infty\}$ by

$$A_s(\boldsymbol{x}) = \left[\sum_{|\boldsymbol{\alpha}|=1}^{s+2} \sum_{|\boldsymbol{\beta}|=s+2-|\boldsymbol{\alpha}|} \frac{1 + \delta_{0,|\boldsymbol{\beta}|}}{2c^s \boldsymbol{\alpha}! \boldsymbol{\beta}!} \left| Z_h^{\boldsymbol{\alpha}+\boldsymbol{\beta}}(\boldsymbol{x}) - Y^{\boldsymbol{\alpha}+\boldsymbol{\beta}} \right| \right]^{-1}, \quad -1 \leq s < r,$$

$$A_r(\boldsymbol{x}) = \left[\sum_{|\boldsymbol{\alpha}|=1}^{r+2} \sum_{|\boldsymbol{\beta}|=r+2-|\boldsymbol{\alpha}|} \frac{1 + \delta_{0,|\boldsymbol{\beta}|}}{2\boldsymbol{\alpha}! \boldsymbol{\beta}!} c^{n+2} \sum_{p \in \mathcal{N}(\boldsymbol{x})} \left| \frac{v_p}{h^n} \left(\frac{\boldsymbol{x} - \boldsymbol{x}_p}{h} \right)^{\boldsymbol{\alpha}+\boldsymbol{\beta}} \eta \left(c \frac{\boldsymbol{x} - \boldsymbol{x}_p}{h} \right) \right| \right]^{-1}, \tag{3.6}$$

an upper bound on the approximation error

$$E(\boldsymbol{x}) = |Q_h f(\boldsymbol{x}) - Lf(\boldsymbol{x})| \tag{3.7}$$

of the PSE operator in (2.2) can be expressed from (3.3)–(3.4) as

$$E(\boldsymbol{x}) \leq \sum_{s=-1}^{r} \frac{h^s}{A_s(\boldsymbol{x})} \|f\|_{W^{s+2,\infty}(B_{r_c}[\boldsymbol{x}])} \|\nu\|_{W^{s+1,\infty}(B_{r_c}[\boldsymbol{x}])}. \tag{3.8}$$

Each $A_s(\boldsymbol{x})$, $s \leq r$, hence quantifies the accuracy of Q_h at order s. We thus call A_s the *accuracy measures* for the PSE operator. Under the reasonable assumption that refinement is performed such that the distances between particles scale with the spatial resolution h, and the volumes with h^n, it is clear that the accuracy measures are independent of h.

For DC PSE operators [31], the kernel η is constructed such that its discrete moments from (3.5) satisfy

$$Z_h^{\boldsymbol{\alpha}} = Y^{\boldsymbol{\alpha}}, \ |\boldsymbol{\alpha}| < r + 2, \tag{3.9}$$

where

$$Y^{\boldsymbol{\alpha}} = \begin{cases} 2, & \boldsymbol{\alpha} = 2\boldsymbol{e}_i, \ i = 1, \ldots, n, \\ 0 & \text{else.} \end{cases}$$

In this case, $A_s(\boldsymbol{x}) = \infty \ \forall s < r$ and the truncation error in (3.8) is truly of order r. Only $A_r(\boldsymbol{x})$ is then relevant.

For uncorrected (UC) PSE operators, the kernel η is constructed to satisfy the *continuous* moment conditions

$$c^{n+2} \int_{\mathbb{R}^n} \boldsymbol{z}^{\boldsymbol{\alpha}} \eta(\boldsymbol{z}) d\boldsymbol{z} = Y^{\boldsymbol{\alpha}}, \ |\boldsymbol{\alpha}| < r + 2\,. \tag{3.10}$$

In this case, $A_s(\boldsymbol{x})$ is not necessarily infinite for $s \leq r$ and, in general, most of the terms in (3.8) do not vanish. Whether error terms with $s < r$ can be neglected (in which case the truncation error *appears* to be of order r) or not depends on the resolution h and on the fields f and ν. The error magnitude at each order s, however, can be estimated a priori from $A_s(\boldsymbol{x})$, $s \leq r$.

Similarly, the influence of a PSE operator on the stability of a time-discretized diffusion scheme can be separated from problem-dependent parameters. Therefore, consider the semidiscrete equation

$$\frac{\partial f(\boldsymbol{x},t)}{\partial t} = Q_h f(\boldsymbol{x},t) \tag{3.11}$$

and discretize the time derivative using (for example) a forward Euler difference scheme

$$f(\boldsymbol{x},t+\Delta t) = f(\boldsymbol{x},t) + \Delta t\, Q_h f(\boldsymbol{x},t).$$

The dispersion relation for a wave $g(\boldsymbol{x},t) = \exp\left(\hat{\imath}(\boldsymbol{k}\cdot\boldsymbol{x} - \omega t\nu/h^2)\right)$ that satisfies the semidiscrete (3.11) is

$$\omega(\boldsymbol{k}) = \hat{\imath}c^{n+2}\sum_{p\in\mathcal{N}(\boldsymbol{x})}\frac{v_p}{h^n}\left[\exp\left(\hat{\imath}\boldsymbol{k}\cdot(\boldsymbol{x}_p-\boldsymbol{x})\right)-1\right]\eta\left(c\frac{\boldsymbol{x}-\boldsymbol{x}_p}{h}\right)$$

and a von Neumann stability analysis reveals that the bound on the time step guaranteeing exponential stability for all wavenumbers $\boldsymbol{k}$ is

$$\Delta t < S\frac{h^2}{\nu}, \tag{3.12}$$

where

$$S = \inf_{|\boldsymbol{k}|\in]0,\sqrt{n}\pi/h]}\left\{\frac{-2\,\mathrm{Im}(\omega(\boldsymbol{k}))}{|\omega(\boldsymbol{k})|^2}\right\}. \tag{3.13}$$

The scalar S thus characterizes the stability of the PSE operator, as it can be used to derive the admissible time-step size for given problem-dependent parameters (here, h and ν) from (3.12). The measure S itself, however, is problem-independent.

4. Operator quality measures. We formalize and generalize the ideas presented in the previous section by introducing a set of three problem-independent quality measures that quantify the characteristics of different operators or different operator parameter settings along three dimensions: accuracy, stability, and computational cost. These measures allow one to compare different operators and study the effects of their free parameters. We demonstrate this in section 5, where we present a full parameter study for PSE diffusion operators, constructing their parameter landscapes exclusively from the quality measures introduced here. In section 6 we show how these quality measures can be used to construct predictive performance models that allow one to automatically choose the best operator for a given problem at hand.

We derive measures for the following characteristics of any particle diffusion operator:

1. its accuracy,
2. its stability in explicit time stepping, and
3. its computational cost.

We call the measures introduced here problem-independent because they do not depend on problem parameters such as the viscosity field ν or the field f to which the operator is applied. Nor do they depend on any numerical parameters, such as the spatial or temporal resolution. Since the measures do, however, depend on the spatial distribution of the particles, we assume that the rescaled positions $(\boldsymbol{x}_p-\boldsymbol{x})/h$ of the particles $\boldsymbol{x}_p$ in the neighborhood of a point $\boldsymbol{x}$ and the rescaled volumes v_p/h^n are independent of h (i.e., they are scale invariant). This is a reasonable assumption, as otherwise one would use adaptive refinement techniques to restore this property.

4.1. Quantifying accuracy. Following the error analysis presented in section 3 we define the problem-independent accuracy measures $A_s(\boldsymbol{x}) \in \mathbb{R}^+ \cup \{\infty\}$, $s \leq r$, such that the overall error

$$E(\boldsymbol{x}) = |Q_h f(\boldsymbol{x}) - Lf(\boldsymbol{x})| \tag{4.1}$$

is bounded by

$$E(\boldsymbol{x}) \leq \sum_{s=-2}^{r} \frac{h^s}{A_s(\boldsymbol{x})} \|f\|_{W^{s+2,\infty}(B_{r_c}[\boldsymbol{x}])} \|\nu\|_{W^{s+1,\infty}(B_{r_c}[\boldsymbol{x}])}. \tag{4.2}$$

From this, the A_s are not uniquely defined. This is for practical reasons, since tight bounds for (4.2) are not always available.

For the anisotropic case, we replace the norm $\|\nu\|_{W^{m,\infty}(\Omega)}$ in (4.2) by

$$\sup_{\substack{0 \leq |\boldsymbol{\alpha}| \leq m \\ \boldsymbol{y} \in \Omega}} \|D^{\boldsymbol{\alpha}} \boldsymbol{\nu}(\boldsymbol{y})\|_{\mathrm{F}},$$

where $\|\cdot\|_{\mathrm{F}}$ denotes the Frobenius norm.

The accuracies $A_s(\boldsymbol{x})$, $s < r$, should be large compared to $A_r(\boldsymbol{x})$, such that error terms of order $s < r$ are negligible even for small h. If this is the case, a larger $A_r(\boldsymbol{x})$ implies a lower upper bound on the error at position $\boldsymbol{x}$.

Closed-form expressions for the measures A_s are given in Appendix A for the anisotropic PSE diffusion operator, the Fishelov diffusion operator, the diffusion operator of a resampling method, and a robust diffusion operator used in SPH. The A_s for isotropic PSE operators are derived in section 3.

4.2. Quantifying stability. In order to quantify the influence of a discretized diffusion operator on the von Neumann stability in explicit time stepping, we define a problem-independent stability measure S such that the time-step limit in an explicit Euler scheme for solving

$$\frac{\partial f(\boldsymbol{x}, t)}{\partial t} = Q_h f(\boldsymbol{x}, t) \tag{4.3}$$

is given by

$$\Delta t < S \frac{h^2}{\nu}. \tag{4.4}$$

That is, the CFL number $\alpha_{\mathrm{CFL}} = \Delta t \nu / h^2$ must be smaller than S if the corresponding operator is used in explicit Euler time stepping. The stability S also indicates trends of the time-step limit when using other explicit methods for time integration. When using Heun's method, for example, the time-step limit is increasing with increasing S (for $S > 0$), but the relationship is not linear and depends on additional characteristics of the operator. If necessary, analogous stability measures can also be derived for other explicit time stepping methods from a von Neumann stability analysis.

Closed-form expressions for the stability measures S of different diffusion operators are again given in Appendix A. They are derived assuming constant (homogeneous) viscosity.

4.3. Quantifying computational cost. We define

$$C = V_n \left(\frac{r_c}{h}\right)^n \tag{4.5}$$

as a problem-independent measure of the computational cost of an operator. Here, V_n is the volume of the n-dimensional unit ball and r_c is the radius of the operator support ("cutoff radius"). Thus, the measure C merely approximates the number of neighbors of each particle. We do not account for the cost of computing the weights of the operator evaluations since look-up tables are commonly used to avoid these function evaluations. Also, the construction of the operator itself is not taken into account because in many applications it is done just once in the beginning of a simulation.

5. Influence of free operator parameters on the quality of PSE operators. We demonstrate how the above operator quality measures can be used to determine good values for an operator's free parameters, without having to run any benchmark simulations. We do this in a parameter study for UC [9] and DC [31] PSE diffusion operators.

The PSE diffusion operator $Q_h(\cdot)$ defined in (3.1) is determined by the choice of the kernel function η, the cutoff radius r_c, and the ratio $c = h/\varepsilon$. One objective here is to demonstrate the influence of these parameters on the operator's properties, providing a guideline for their choice in practice. Based on the quality measures introduced in section 4, we construct the parameter landscapes ("phase diagrams") of PSE operators. The parameters are described in section 5.1 and the results of the parameter study are presented in section 5.2.

The quality measures presented in section 4 depend on the underlying spatial distribution of particles. For simplicity, we restrict the present study to uniform Cartesian particle distributions as they are obtained, e.g., by remeshing [18]. Also, we only consider operators used for three-dimensional simulations with isotropic viscosity. The quality measures introduced above, however, are equally valid in the general case, i.e., in any number of dimensions and for any particle distribution, as we show in section 6.

5.1. PSE operator parameters. We first describe the free parameters of PSE diffusion operators and state the ranges within which they are varied in the subsequent parameter study.

5.1.1. The kernel function. One of the parameters of the operator is the kernel function η. Any kernel that satisfies the moment conditions as outlined in section 3 and in Appendix A.1 leads to a consistent approximation, but the error magnitude may vary with kernel shape. Here, we focus on kernel functions of the form

$$\eta(\boldsymbol{z}) = K(z)\phi(z), \quad z = |\boldsymbol{z}| = \left[\sum_{k=1}^{n} z_k^2\right]^{1/2}, \tag{5.1}$$

where K is called the correction function and ϕ the window function. We consider ϕ and K free parameters of the diffusion operator and test the following possible choices:

$$\begin{aligned}
&\phi_1(z) = \exp\left(-z^2\right), && \phi_2(z) = \frac{1}{z^{10}+1},\\
&\phi_3(z) = \frac{1}{(1+z^2)^5}, && \phi_4(z) = \operatorname{sech}(z),\\
&\phi_5(z) = z\operatorname{cosech}(z), && \phi_6(z) = \exp\left(-z^2\right)\cos(\sqrt{2}z),\\
&\phi_7(z) = \frac{1}{\pi}\sin(\pi z)/\sinh(z), && \phi_8(z) = \begin{cases}\exp\left(\frac{1}{z^2-R^2}+\frac{1}{R^2}\right), & z<R,\\ 0 & \text{else},\end{cases}\\
&\phi_9(z) = \begin{cases}1, & z<R,\\ 0 & \text{else},\end{cases} && \phi_{10}(z) = \begin{cases}(R-z)/R, & z<R,\\ 0 & \text{else}\end{cases}
\end{aligned} \tag{5.2}$$

and

$$\begin{aligned}
&K_1(z) = \sum_{k=0}^{m-1} a_k z^k, && K_2(z) = \sum_{k=0}^{m-1} a_k z^{2k},\\
&K_3(z) = \sum_{k=0}^{m-1} a_k \cos(kz), && K_4(z) = a_0 + \sum_{k=1}^{m-1} a_k \sin(kz).
\end{aligned} \tag{5.3}$$

Via the coefficients a_k, the correction functions K have m degrees of freedom. The number m corresponds to the number of moment conditions that are not automatically fulfilled by symmetry. The coefficients a_k are determined such that the moment conditions in (3.9) or (3.10) are satisfied for DC and UC PSE operators, respectively. For UC operators, we only consider the correction function K_2.

Since the number of moment conditions depends on the desired order of accuracy r, the number m of coefficients a_k in a correction function K also depends on r. The choice of the kernel function hence implies a choice of the order of accuracy r. For second-order accurate operators ($r = 2$), $m = 1$. In this case, the correction functions K_1 to K_4 are identical and we will in the following omit their specification.

The above selection of window functions ϕ is motivated by the kernel functions proposed by Cottet and Koumoutsakos [6] (ϕ_1 to ϕ_3) and Maz'ya and Schmidt [23] (ϕ_4 to ϕ_7). The window functions ϕ_8 to ϕ_{10} are included for their simplicity and compact support. We always use $R = 3$. The ten window functions tested are plotted in Figure 5.1.

5.1.2. The cutoff radius. The second parameter of a PSE operator is the cutoff radius r_c, which defines the size of the neighborhood of a particle at position $\boldsymbol{x}$. Reducing the cutoff radius reduces the cost of operator evaluation, as fewer particles are considered neighbors and the sum over neighboring particles in (3.1) is shorter. For UC operators, however, reducing the cutoff radius increases the discretization error, because the approximated integral is truncated [31]. A large cutoff radius is expected to increase operator stability and decrease its sensitivity to perturbations in the particle positions.

We render this parameter independent of the spatial resolution by normalizing it with the kernel width ε as r_c/ε. This is typically how r_c is scaled in particle simulations. The minimum admissible cutoff radii are $r_{c,\min}/\varepsilon = c$ for order $r = 2$ and $r_{c,\min}/\varepsilon = 2c$ for order $r = 4$. Smaller cutoff radii cannot be used since the number

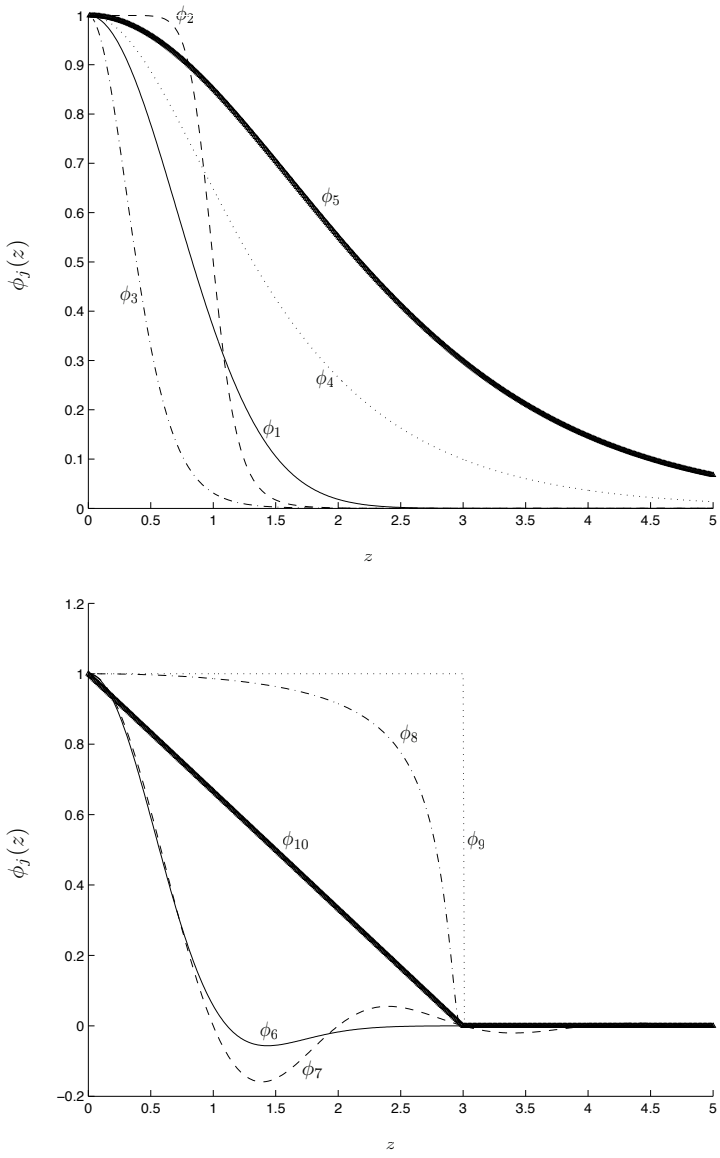

FIG. 5.1. *The ten window functions from* (5.2).

of particles contained in the ball $B_{r_c}[\boldsymbol{x}]$ would be too small to yield an rth-order approximation. We test a set $R_c = \{r_{c,1} = r_{c,\min}, r_{c,2}, \ldots, r_{c,k} = r_{c,\max}\}$, $r_{c,i} < r_{c,i+1}$, of cutoff radii, where the differences $r_{c,i+1} - r_{c,i}$ are minimized under the constraint that the number of particles in $B_{r_{c,i}}[\boldsymbol{x}]$ is different from the number of particles in $B_{r_{c,i+1}}[\boldsymbol{x}]$. The maximum cutoff radii $r_{c,\max}$ considered here depend on the order of accuracy r and on the window function ϕ as listed in Table 5.1.

5.1.3. The ratio $c = h/\varepsilon$. The third free parameter of a PSE operator is the ratio c. For constant r_c/ε, a small ratio $c = h/\varepsilon$ reduces the difference between the discrete moments in (3.5) and the continuous moments in (3.10). Small c therefore

TABLE 5.1
The maximum normalized cutoff radii $r_{c,\max}/\varepsilon$ considered for the different window functions in the present parameter study.

	ϕ_1	ϕ_2	ϕ_3	ϕ_4	ϕ_5	ϕ_6	ϕ_7	ϕ_8	ϕ_9	ϕ_{10}
$r=2$	5	10	10	10	10	10	5	3	3	3
$r=4$	7	12	12	12	12	12	7	3	3	3

typically improve the accuracy of UC PSE operators. The cost of operator evaluation, however, is larger for smaller c, since more particles are located in the neighborhood of $\boldsymbol{x}$. The accuracy of DC PSE operators is expected to be higher for larger c: the influence of the direct neighbors relative to the influences of more distant particles is typically higher because the window function is more peaked and less smoothing occurs. The values of c tested here are $\{0.25, 0.3, 0.35, \ldots, 1.4\}$.

5.2. Parameter study results. We evaluate all possible combinations of the operator parameters listed above by computing the corresponding quality measures for both DC and UC PSE diffusion operators on uniform Cartesian particle distributions. Since the quality measures are explicitly known, all 443,956 parameter combinations can rapidly be tested. If one were to run a benchmark simulation for each parameter set, this would clearly be infeasible. Below, we summarize the results of the parameter study in the form of "phase diagrams" of the operator's parameter space, and we point out potential trade-offs in the parameter choices.

The cost measure C is by definition independent of K and ϕ and hence depends only on the cutoff radius r_c relative to the interparticle spacing h. Since it does not depend on K, the cost C is identical for both UC and DC operators, as shown in Figures 5.2 and 5.3. In the region where $r_c/\varepsilon < c$ or $r_c/\varepsilon < 2c$ for $r = 2$ or $r = 4$, respectively, there are not enough particles in the closed ball $B_{r_c}[\boldsymbol{x}]$. The number of neighbors around $\boldsymbol{x}$ is then too small and there is not enough information to approximate $Lf(\boldsymbol{x})$ with the desired order of accuracy. The minimum possible cost is $C = V_3$ (i.e., the volume of the three-dimensional unit ball) for $r = 2$ and $C = 8V_3$ for $r = 4$ on the lines $r_c/\varepsilon = c$ and $r_c/\varepsilon = 2c$, respectively.

Typical landscapes of the other quality measures of UC and DC PSE operators over r_c/ε and c are also shown in Figures 5.2 and 5.3. The salient features of these landscapes are preserved across window and correction functions, allowing us to generalize the results. The resulting sketch diagram for the cost measure is shown in Figure 5.4; those for the other quality measures are shown in Figures 5.5 and 5.6 for UC and DC PSE operators, respectively.

For a fixed cutoff r_c/ε, UC PSE operators do not converge for increasing resolution [31]. This is because error terms of order $s < r$ do not necessarily vanish. For certain ranges of resolution, however, it can be that $h^s/A_s \ll h^r/A_r \;\forall\; s < r$, guaranteeing apparent rth-order convergence (see (4.2)). For these resolutions, UC PSE operators can still be used in practice. Given this restriction on A_s, and hence the choice of r_c and c, the user can choose an operator with a reasonable time-step stability limit. However, the cost of operator evaluation will be high and the accuracy A_r low.

For DC PSE operators, the accuracy measures A_s, $s < r$, are by definition infinitely large whenever enough neighboring particles are present. In practice, where numerical errors are introduced when constructing the operators (i.e., computing the weights of the kernels), the accuracy measures are finite, but much larger than A_r

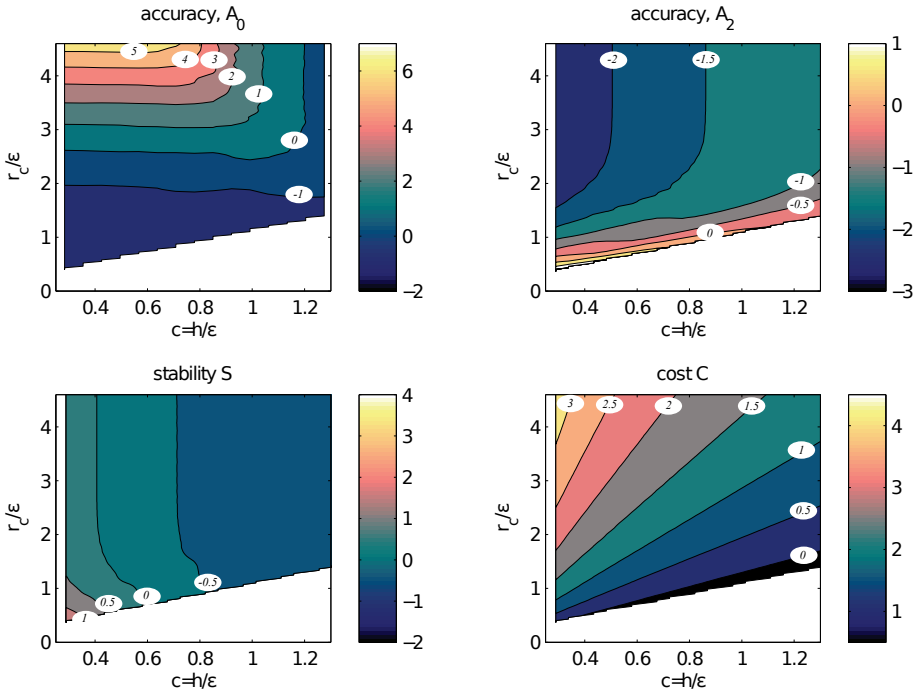

FIG. 5.2. *Quality measure landscapes for UC PSE diffusion operators with* $r = 2$ *and the Gaussian kernel* ϕ_1*; shading codes the* $\log_{10}$ *of each measure's value.*

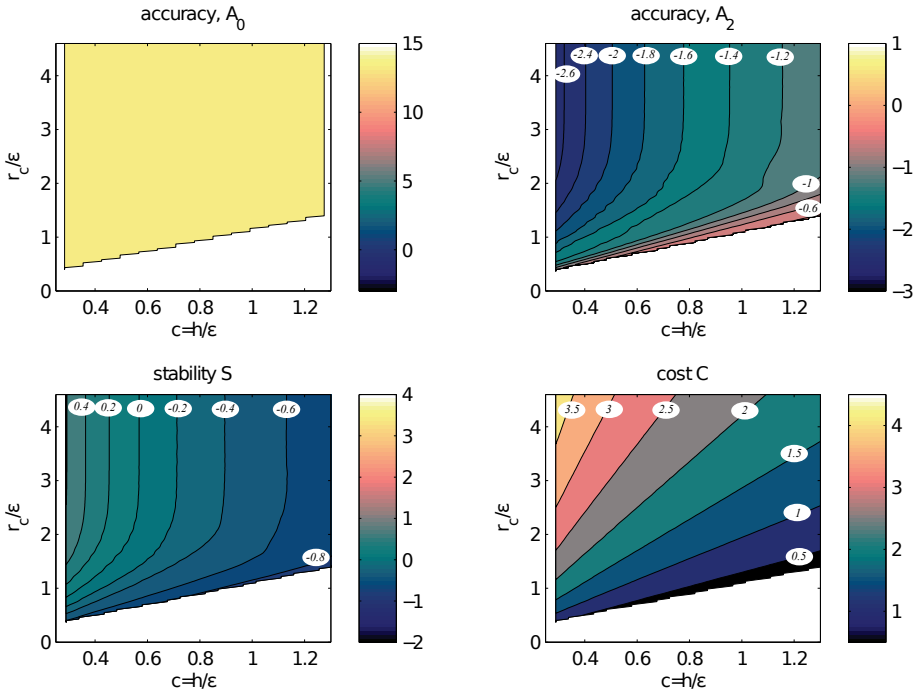

FIG. 5.3. *Quality measure landscapes for DC PSE diffusion operators with* $r = 2$ *and the Gaussian kernel* ϕ_1*; shading codes the* $\log_{10}$ *of each measure's value.*

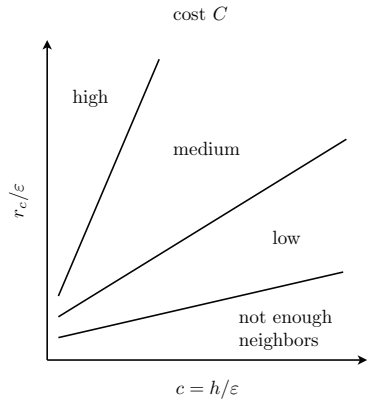

FIG. 5.4. *Sketch of the cost measure's dependence on the cutoff radius and the ratio c.*

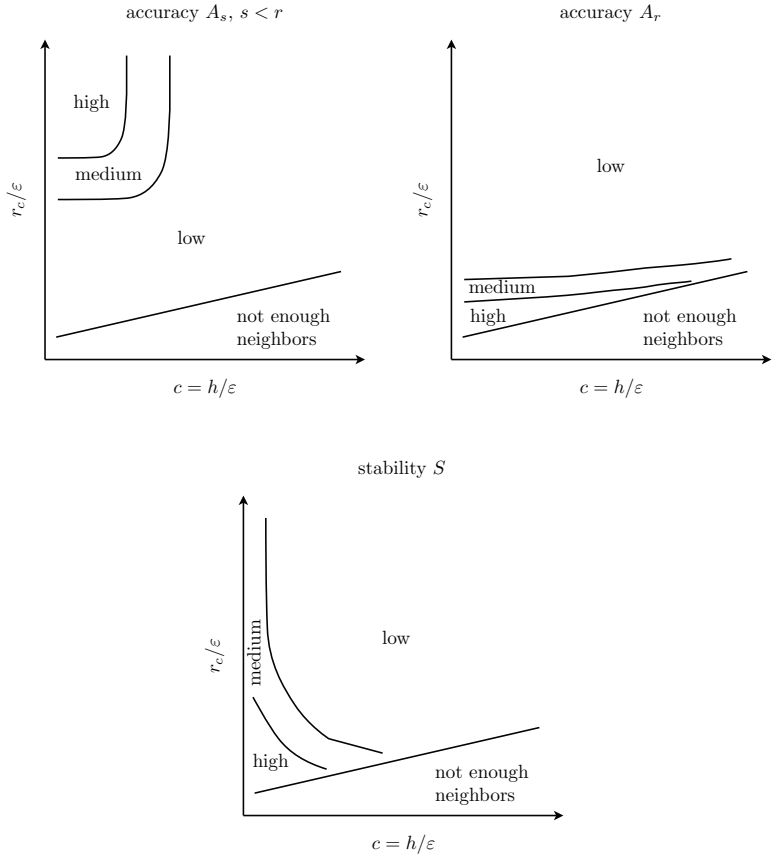

FIG. 5.5. *Sketches of the quality measure landscapes for UC PSE diffusion operators.*

such that they usually do not influence the choice of r_c and c. If accuracy is the only criterion for operator design, the choice of r_c and c is simple: for decreasing $r_c/(c\varepsilon)$, the accuracy A_r increases and the cost C decreases, such that r_c and c should be chosen on the line $r_c/\varepsilon = c$ or $r_c/\varepsilon = 2c$ for $r = 2$ or $r = 4$, respectively. For second-order

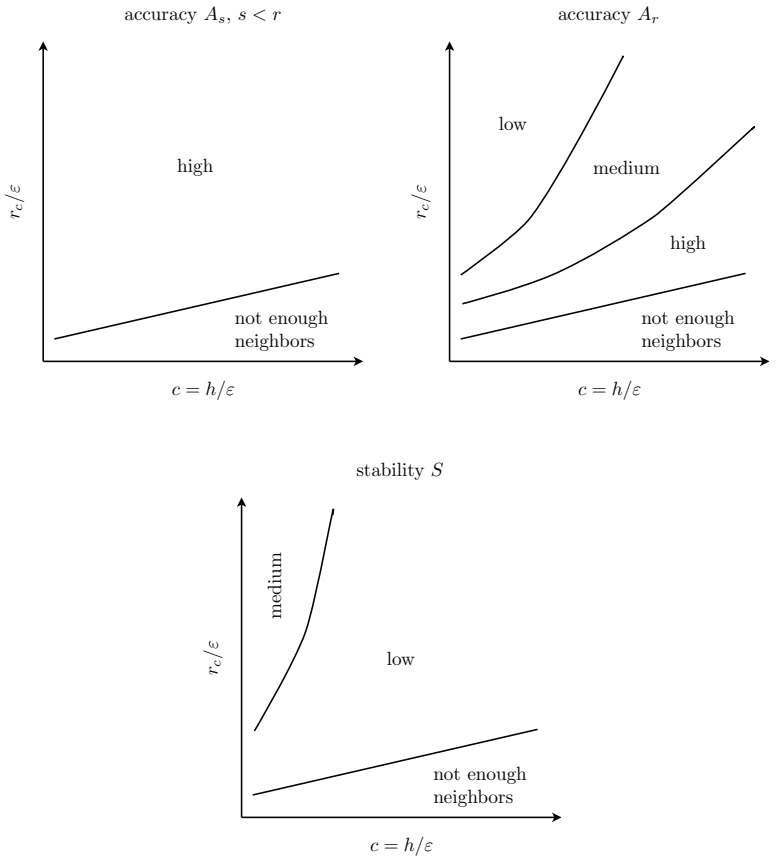

FIG. 5.6. *Sketches of the measure landscapes for DC PSE diffusion operators.*

accurate operators, the choice of c is in this case arbitrary, because all operators with $r_c/\varepsilon = c$ (for any window function ϕ) reduce to the classical finite-difference (FD) stencil

$$Q_h f(\boldsymbol{x}) \;=\; \frac{\nu}{h^2} \sum_{i=1}^{n} [f(\boldsymbol{x} + \boldsymbol{h}_i) - 2f(\boldsymbol{x}) + f(\boldsymbol{x} - \boldsymbol{h}_i)]$$

if ν is constant, or

$$\begin{aligned} Q_h f(\boldsymbol{x}) = \frac{1}{2h^2} \sum_{i=1}^{n} \{ & [f(\boldsymbol{x} + \boldsymbol{h}_i) - f(\boldsymbol{x})][\nu(\boldsymbol{x}) + \nu(\boldsymbol{x} + \boldsymbol{h}_i)] \\ & + [f(\boldsymbol{x} - \boldsymbol{h}_i) - f(\boldsymbol{x})][\nu(\boldsymbol{x}) + \nu(\boldsymbol{x} - \boldsymbol{h}_i)] \} \end{aligned} \tag{5.4}$$

else, where $\boldsymbol{h}_i$ is a vector of length h pointing along dimension i. The fourth-order accurate operators on the line $r_c/\varepsilon = 2c$ generally vary with c and are different for different choices of the window function ϕ and the correction function K. Therefore, the choices of ϕ, K, and c influence A_r. If accuracy is not the only important criterion, choosing ϕ, K, r_c, and c is more difficult. As can be seen from Figures 5.3 and 5.6, highly accurate operators typically require small time-step limits for stable explicit time stepping. On the other hand, a larger stability measure S requires a more costly operator of comparably low accuracy. A trade-off must hence be found.

6. Real-world applicability and interplay of the quality measures: A case study. In practice, the most interesting property of an operator is probably the computational time needed to solve a given problem with a certain maximum error. This property may depend on all three quality measures introduced in section 4, and while their values do not depend on the problem to be solved, their relative influences do.

We now show how the introduced quality measures can be used for identifying a predictive performance model—an a posteriori runtime estimate—and for choosing the best operator and operator parameters for a given problem. This is based on a small number of problem-specific benchmark simulations from which one can infer the interplay and individual importance of the quality measures. This can be seen as "calibrating" the performance model given by the quality measures to a specific problem, hardware, implementation, compiler, etc., and hence accounts for all of these influences on the expected runtime. This also means that the calibration benchmarks have to be redone every time one of these conditions changes. The quality measures provide an a priori idea of how the cost scales with operator parameters, which is independent of the hardware and compiler used. The a posteriori runtime model identified from the benchmarks can then be used to select the most suitable operator for the given problem at hand, leading to significant computational savings.

As a test case we use the three-dimensional advection-diffusion problem described in Appendix B. We consider two variants of this problem: (i) simulations where the particles are remeshed after every time step, such that the particle distribution always remains uniformly Cartesian when the diffusion operator is applied; (ii) simulations where the intervals between remeshing events are large, hence leading to irregular and distorted particle distributions. All benchmarks are implemented in Fortran 90, compiled using the Intel Fortran Compiler version 11 with optimization flag `-O3`, and run on an Intel CoreDuo 2 with 2 GB RAM.

6.1. Advection-diffusion simulation with remeshing at every time step. We consider the three-dimensional advection-diffusion problem of Appendix B, solved with remeshing at every time step. For remeshing, we use the third-order accurate M_4' kernel as given in (B.1). We perform a small number of 13 timing benchmarks in order to calibrate the cost measure C to CPU wall-clock time in seconds using linear regression, as shown in Figure 6.1. When remeshing at every time step, the calibration curve estimates that the CPU time needed for one time step of the simulation is approximately

$$C_{\mathrm{UC}} = C_{\mathrm{DC}} \approx 0.20 + 0.0035C\,,$$

where C is the cost measure of the diffusion operator used. Assuming that for efficiency reasons we want to use the largest time step possible, the CPU time needed for the complete simulation is proportional to $C_{\mathrm{UC/DC}}/S$. Thus, an efficient operator for this simulation should have a low ratio

$$F = \frac{0.20 + 0.0035C}{S}$$

under the constraint that it has a zeroth-order accuracy A_0 of more than 10^7 and a

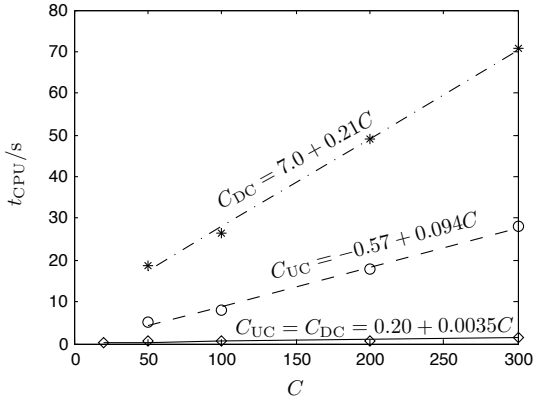

FIG. 6.1. *Calibration timing experiments. We show the relationship between the cost measure C and the CPU time t_{CPU} for $h = 0.217$ and $\Delta t = 0.0125$ when remeshing at every time step (UC/DC: $\diamond$) or remeshing at large time intervals (UC: $\circ$, DC: $*$). We fit t_{CPU}/s with the functions $C_{UC}(C)$ and $C_{DC}(C)$, respectively, using linear regression.*

positive stability measure S.[1] We do not account for the accuracy measures A_s, $s > 0$, because the remeshing error dominates and masks these higher-order errors of the diffusion operator.

The operator that meets these constraints with the lowest ratio F is the DC PSE operator with $r = 2$, ϕ_7, $c = 0.6$, and $r_c/\varepsilon = 1.47$. We call this the *appointed operator* in the following and compare its performance to six other operators that are frequently used for advection-diffusion problems. Two of these operators are the FD stencils of (5.4) and

$$\begin{aligned} Q_h f(\boldsymbol{x}) = \frac{1}{24h^2} \sum_{i=1}^{n} \{ & [\nu(\boldsymbol{x} - 2\boldsymbol{h}_i) + \nu(\boldsymbol{x})][f(\boldsymbol{x}) - f(\boldsymbol{x} - 2\boldsymbol{h}_i)] \\ & + 16[\nu(\boldsymbol{x} - \boldsymbol{h}_i) + \nu(\boldsymbol{x})][f(\boldsymbol{x} - \boldsymbol{h}_i) - f(\boldsymbol{x})] \\ & + 16[\nu(\boldsymbol{x} + \boldsymbol{h}_i) + \nu(\boldsymbol{x})][f(\boldsymbol{x} + \boldsymbol{h}_i) - f(\boldsymbol{x})] \\ & + [\nu(\boldsymbol{x} + 2\boldsymbol{h}_i) + \nu(\boldsymbol{x})][f(\boldsymbol{x}) - f(\boldsymbol{x} + 2\boldsymbol{h}_i)] \} \end{aligned} \tag{6.1}$$

of orders $r = 2$ and $r = 4$, respectively. The four other operators are second- and fourth-order DC and UC PSE operators with large[2] cutoff radii and medium c, as recommended by "best practice" for UC PSE operators. For each operator, we adjust h and Δt semiautomatically such that the CPU time is low and the maximum error does not exceed a certain target error level $E^*_{\max}$ at final simulation time $T = 0.25$. All simulations take advantage of the consistently uniform Cartesian distribution of particles: particles are identified by mesh indices and no neighbor lists (cell list or Verlet lists [33]) are used in these simulations. The results are given in Table 6.1. As predicted by the performance model, the appointed operator performs best. In

[1] The value 10^7 is chosen arbitrarily, and any value in $[0.6, 10^{15}]$ leads to the same result. This can be explained from the quality measure landscapes shown in Figures 5.2 and 5.3: medium values of A_0 are associated with large costs C and low or medium values of S, such that operators with $A_0 \in [0.6, 10^{15}]$ correspond to large F. The stability measure S is required to be positive for explicit time stepping to be stable.

[2] The cutoff radii of $r_c = 3.5\varepsilon$ and $r_c = 5.5\varepsilon$ for the second- and fourth-order accurate operators, respectively, are large compared to those of the FD stencils and of the appointed operator.

TABLE 6.1

Advection-diffusion simulations with remeshing at every time step. We report the shortest[a] *CPU times for solving the test case to two different target error levels* $E^*_{\max} = \{0.05, 0.01\}$. *We show the results for six typical diffusion operators, sorted by descending CPU times, and for the appointed operator (shaded entry).*

$E^*_{\max} = 0.05$

	r	c	r_c/ε	h	Δt	t_{CPU} in s
DC, ϕ_1, K_2	4	0.9	5.5	0.370	0.0417	0.208
UC, ϕ_1, K_2	4	0.9	5.5	0.370	0.0417	0.207
fourth-order FD (6.1)				0.349	0.0278	0.0555
DC, ϕ_1	2	0.9	3.5	0.331	0.0625	0.0442
UC, ϕ_1	2	0.9	3.5	0.331	0.0625	0.0421
second-order FD (5.4)				0.349	0.0417	0.0223
DC, ϕ_7	2	0.6	1.47	0.370	0.125	0.00950

$E^*_{\max} = 0.01$

	r	c	r_c/ε	h	Δt	t_{CPU} in s
UC, ϕ_1, K_2	4	0.9	5.5	0.185	0.00556	13.2
DC, ϕ_1, K_2	4	0.9	5.5	0.185	0.00556	13.0
fourth-order FD (6.1)				0.185	0.00287	3.55
second-order FD (5.4)				0.242	0.00417	0.637
DC, ϕ_1	2	0.9	3.5	0.273	0.0208	0.264
UC, ϕ_1	2	0.9	3.5	0.273	0.0208	0.257
DC, ϕ_7	2	0.6	1.47	0.251	0.0417	0.113

[a]Considering the CPU time a function of h and Δt, we report the minimum CPU time and the corresponding values of h and Δt under the constraint of staying below the target error level.

fact, the simulation using the appointed operator completes more than twice as fast as the fastest simulation using any of the other operators. Note that the DC and UC PSE operators with the same parameters lead to the same results here. This is because r_c/ε is large enough and c is small enough for the UC PSE operators to be able to reach the target error level on Cartesian particle distributions. The fourth-order accurate operators perform worst. This can be explained by the fact that the remeshing procedure is of lower order, and the advantage of the high-order accuracy is not exploited in these simulations. Yet the operator evaluation is more costly due to the larger cutoff radii required.

For a target error level of $E^*_{\max} = 0.05$, the second-order FD operator outperforms the two PSE operators listed first. This is not surprising since its cost C is much lower (4.19 vs. 246).[3] The cost C of the appointed operator is higher than the cost of the FD operator (61.6 vs. 4.19). The stability S of the appointed operator, however, is

[3]From the parameter study presented in section 5 we see that the accuracy of the second-order FD operator is the highest of all operators tested. We do, however, consider this effect to be marginal due to the dominance of the remeshing error.

much higher than that of the FD operator, such that a larger time step can be used. In the present case, this is enough to compensate for the higher cost of the operator evaluation. It is, however, important to notice that the quality measures presented here will always appoint the operator that has the highest predicted performance, such that the user does not need to worry about these trade-offs and their causes.

For the target error level $E^*_{\max} = 0.01$, the second-order FD operator is outperformed by all tested second-order PSE operators. The reason is the low time stepping stability of the FD operator, which becomes more apparent at higher resolutions. Again, the high stability of the appointed operator, combined with its lower cost, renders it more efficient than the other operators.

6.2. Advection-diffusion simulation with remeshing at large intervals. If remeshing is performed only at large time intervals, we expect the diffusion error to dominate. We therefore modify the objective function F to represent the influence of the operator accuracy A_r on the CPU time required to solve the given problem to a target error level $E^*_{\max}$: we assume a maximum simulation error $E_{\max} \sim h^r/A_r$. In this case, an interparticle spacing h proportional to $A_r^{1/r}$ is required. Since the number of particles is proportional to h^{-n}, $n = 3$, and the number of time steps to h^{-2}, the factor $A_r^{-5/r}$ is introduced into F. Thus, including the results of the calibration experiments shown in Figure 6.1,

$$F = \frac{-0.57 + 0.094C + \mathbb{I}_{\mathrm{DC}}(7.57 + 0.116C)}{SA_r^{5/r}},$$

where $\mathbb{I}_{\mathrm{DC}} = 1$ for DC PSE operators and $\mathbb{I}_{\mathrm{DC}} = 0$ for UC ones. Note that the influence of the discretization correction on the simulation cost is significant when remeshing is done only at large intervals since the kernels have to be recomputed at every time step due to particle movement [31].

We use the same constraints on A_s, $s < r$, and S as in section 6.1. Additionally, we impose a lower bound on the cutoff radii such that all operator neighborhoods contain enough particles at all times: $r_c/h > 2.14$ for $r = 2$ and $r_c/h > 2.52$ for $r = 4$. The cutoff radius $r_c = h$ or $r_c = 2h$, leading to compact FD stencils, is thus not included. From the parameter study presented in section 5, the second-order DC operator with window function ϕ_2, ratio $c = 1.4$, and cutoff radius $r_c/\varepsilon = 3.2$ is predicted to perform best. We remark, however, that the parameter study was based on uniform Cartesian particle distributions, whereas we have irregular distributions here. It is therefore instructive to see how the performance predictions generalize to the present case.

Table 6.2 lists the resolutions and CPU times required to solve the problem using the different operators. We do not consider fourth-order operators in this test case because their simulation costs are predicted to be much higher than those of the second-order operators: the timing experiments shown in Figure 6.1 are done using second-order accurate operators; for fourth-order operators the runtime t_{CPU} is already 696 s for $C = 100$, due to the higher costs of setting up and solving the linear systems of equations resulting from the discrete moment conditions in (3.9). We thus show the results for two typical second-order accurate PSE operators, and for the appointed operator.

The appointed operator outperforms the other two operators tested by a factor of five to eight. We conclude from this that the performance model based on the quality measures for uniform Cartesian particle distributions is also useful on irregularly distributed particles. Interestingly, the nonappointed DC PSE operator requires a

TABLE 6.2

Advection-diffusion simulations with remeshing at large intervals. We report the shortest[a] *CPU times for solving the test problem to target error levels* $E^*_{\max} = \{0.05, 0.01\}$. *We show the results for two typical PSE diffusion operators and for the appointed operator (shaded entry).*

$E^*_{\max} = 0.05$

	r	c	r_c/ε	h	Δt	t_{CPU} in s
DC, ϕ_1	2	0.9	3.5	0.571	0.125	0.340
UC, ϕ_1	2	0.9	3.5	0.628	0.125	0.104
DC, ϕ_2	2	1.4	3.2	1.05	0.125	0.0196

$E^*_{\max} = 0.01$

	r	c	r_c/ε	h	Δt	t_{CPU} in s
DC, ϕ_1	2	0.9	3.5	0.331	0.0625	3.44
UC, ϕ_1	2	0.9	3.5	0.349	0.050	1.32
DC, ϕ_2	2	1.4	3.2	0.628	0.0625	0.157

[a]Considering the CPU time a function of h and Δt, we report the minimum CPU time and the corresponding values of h and Δt under the constraint of staying below the target error level.

slightly higher resolution than the UC operator to reach the target error level, and it is thus not only more computationally expensive but also less accurate than the UC operator with the same parameters. With the appointed operator, also a DC PSE operator but with a different kernel function and different parameters, the extra computational cost of discretization correction is amortized by the gain in accuracy and the cost reduction due to the smaller neighborhood. This highlights the importance of using the correct kernel function and operator parameters.

Note that the runtimes of the simulations with remeshing at large time intervals (Table 6.2) are longer than those of the simulations where remeshing is done at every time step (Table 6.1). For the simulations using UC PSE operators, the main reason for this is the different implementation: while Verlet lists [33] (as implemented in the PPM Library [30]) are used to find neighbors when particles are irregularly distributed, the particles' mesh-like arrangement is exploited for looking up neighbors in the remeshed case. When using the DC operators, the discretization correction further doubles the computational cost per particle and time step; see Figure 6.1. Rare remeshing, however, is expected to be more efficient for larger Péclet numbers, i.e., for convection-dominated problems (see section 4.4 and Table 2 in [31]).

7. Conclusions and discussion. We proposed three problem-independent quality measures for diffusion operators in particle methods. The measures quantify an operator's accuracy, computational cost, and stability in explicit time stepping. Since they are problem-independent, these operator quality measures can be used to determine good parameter settings for a given operator, or comparing the performance of different operators, without running any benchmark simulations. In the parameter study presented here, this has enabled exhaustively testing 443,956 different operator parameter combinations, which would not have been possible using benchmark simulations. This has allowed us to reconstruct the complete parameter landscapes of the operators, thus visualizing the trade-offs inherent in the operator parameter choices.

The problem-dependent interplay of the quality measures becomes important when constructing predictive performance (runtime) models for a given problem at hand. This can be done by statistical regression over the quality measures from a small number of benchmark simulations. Using only 13 short benchmark runs, we have demonstrated the construction of a predictive performance model for all 443,956 PSE operators, plus a set of common FD operators, which are included as limit cases of DC PSE operators [31]. Using the example of a three-dimensional Lagrangian advection-diffusion simulation, we demonstrated how simple objective functions of the quality measures can predict the expected performance of a wide range of operators and hence help choose efficient ones. Both frequent and occasional remeshing were considered. We demonstrated that an operator's computational efficiency can depend on all three measures. The specific dependence, however, is contingent on the problem to be solved: for problems that are limited in the time-step size by advection rather than by diffusion, the stability measure of the diffusion operator loses its importance. Similarly, the accuracy measure of the diffusion operator might lose importance if frequent remeshing is performed, because the remeshing error then dominates the error introduced by the diffusion operator. If remeshing is a comparably rare event, the operator's accuracy is not negligible. At the same time, however, the most accurate operators typically require small time-step limits, and it might be beneficial to instead use a higher spatial resolution together with an operator of lower accuracy.

The performance model based on the presented quality measures allowed selecting problem-specific operators that were predicted to perform best. We called these operators the *appointed operators* for the given problem. The performance of a given operator on a certain problem is estimated from a small number of benchmark simulations on that problem, calibrating the cost measure to actual CPU time. This calibration curve is valid for all operator parameters, but only for the specific problem (implementation, compiler, hardware) it has been measured on. For a different implementation or computer platform, the performance model needs to be recalibrated. In the case study presented here, reaching a given error level for the solution of the problem was two to eight times faster when using the appointed operators instead of the next best of the tested operators. Once a performance model has been identified for a certain problem, the choice of operator and operator parameters can in principle be automatized in a simulation program. The computational savings demonstrated here are encouraging and we believe that operator performance models will be useful in practice.

We have limited our considerations to diffusion operators in particle methods, which includes compact FD stencils as a limit case. While it is conceivable that a similar approach might also work for other linear differential operators, we do not expect it to easily generalize to nonlinear or integral operators. This is mainly because the a priori error and stability estimates of these operators can be intrinsically problem-dependent, disallowing a separation into problem-independent quality measures and problem-dependent calibration.

Future work will include extending the present framework to more operator types and automating the identification of problem-specific performance models. Also, it shall be interesting to see how the present numerical performance models fit with hardware performance models in order to select the best method or operator for a given problem on a given hardware platform.

Appendix A. Explicit expressions for the quality measures of different diffusion operators. Closed-form expressions for the quality measures introduced in section 4 can be derived for different types of diffusion operators. We exemplify this by

deriving the measures A_s and S for four different operators: PSE diffusion operators, Fishelov diffusion operators, the diffusion operator of a resampling method, and a diffusion operator used in SPH. The cost measure C is universal and does not need to be rederived, as it simply approximates the number of particles used for evaluating $Q_h f(\boldsymbol{x})$. All distances and volumes in this appendix are nondimensionalized using the interparticle spacing h, such that the vectors $\boldsymbol{x} - \boldsymbol{x}_p$ can be considered independent of the spatial resolution. For conciseness, the notation is kept the same.

A.1. PSE diffusion operators. The case of PSE operators with isotropic viscosity was discussed in section 3. Here, we briefly restate PSE operators with anisotropic viscosity [10] and derive their accuracy and stability measures.

The anisotropic diffusion operator $L(\cdot)$ defined in (2.1) is approximated by the PSE operator

$$Q_h f(\boldsymbol{x}) = \frac{c^{n+2}}{\varepsilon^2} \sum_{p \in \mathcal{N}(\boldsymbol{x})} v_p \left(f(\boldsymbol{x}_p) - f(\boldsymbol{x})\right) \eta(c(\boldsymbol{x} - \boldsymbol{x}_p)) \sum_{i,j=1}^{n} \mu_{ij}(\boldsymbol{x}, \boldsymbol{x}_p)(\boldsymbol{x} - \boldsymbol{x}_p)^{\boldsymbol{e}_i + \boldsymbol{e}_j},$$

where

$$\boldsymbol{\mu}(\boldsymbol{x}, \boldsymbol{y}) = \frac{1}{2}\left[\boldsymbol{\nu}(\boldsymbol{x}) + \boldsymbol{\nu}(\boldsymbol{y}) - \frac{\operatorname{tr}(\boldsymbol{\nu}(\boldsymbol{x}) + \boldsymbol{\nu}(\boldsymbol{y}))}{n+2}\boldsymbol{I}\right],$$

and $\boldsymbol{I}$ is the identity matrix in $\mathbb{R}^{n \times n}$.

The moment conditions on the kernel function η for DC or UC operators are

$$Z_h^{\boldsymbol{\alpha}} = Y^{\boldsymbol{\alpha}}, \quad 3 \le |\boldsymbol{\alpha}| < r + 4,$$

with $Z_h^{\boldsymbol{\alpha}}$ defined as in (3.5) and

$$c^{n+2} \int_{\mathbb{R}^n} \boldsymbol{z}^{\boldsymbol{\alpha}} \eta(\boldsymbol{z}) d\boldsymbol{z} = Y^{\boldsymbol{\alpha}}, \quad 3 \le |\boldsymbol{\alpha}| < r + 4,$$

respectively, where

$$Y^{\boldsymbol{\alpha}} = \begin{cases} 1, & \boldsymbol{\alpha} = 2\boldsymbol{e}_i + 2\boldsymbol{e}_j,\ i, j = 1, \ldots, n,\ i \ne j, \\ 3, & \boldsymbol{\alpha} = 4\boldsymbol{e}_i,\ i = 1, \ldots, n, \\ 0 & \text{else.} \end{cases}$$

The accuracy measures for the case of anisotropic viscosity then are $A_{-2}(\boldsymbol{x}) = \infty$ and

$$A_s(\boldsymbol{x}) = \left[\sum_{|\boldsymbol{\alpha}|=1}^{s+2} \sum_{|\boldsymbol{\beta}|=s+2-|\boldsymbol{\alpha}|} \frac{\left(1 + 3\delta_{0,|\boldsymbol{\beta}|}\right) n}{2\boldsymbol{\alpha}!\boldsymbol{\beta}!} \left(\frac{|\operatorname{tr}(\boldsymbol{U})|}{n} + \frac{\lambda^{\boldsymbol{U}}_{\max} - \lambda^{\boldsymbol{U}}_{\min}}{2} + \left|\frac{\operatorname{tr}(\boldsymbol{U})}{n} - \frac{\lambda^{\boldsymbol{U}}_{\max} + \lambda^{\boldsymbol{U}}_{\min}}{2}\right|\right)\right]^{-1}, \ -1 \le s < r,$$

$$A_r(\boldsymbol{x}) = \left[\sum_{|\boldsymbol{\alpha}|=1}^{r+2} \sum_{|\boldsymbol{\beta}|=r+2-|\boldsymbol{\alpha}|} \frac{1 + \delta_{|\boldsymbol{\beta}|,0}}{4\boldsymbol{\alpha}!\boldsymbol{\beta}!} c^{r+2+n} \times \sum_{p \in \mathcal{N}} \operatorname{tr}(\boldsymbol{X}_p) \left| v_p \eta\left(c(\boldsymbol{x} - \boldsymbol{x}_p)\right) (\boldsymbol{x} - \boldsymbol{x}_p)^{\boldsymbol{\alpha}+\boldsymbol{\beta}} \right| \right]^{-1}.$$

The elements of the matrices $\boldsymbol{U}, \boldsymbol{X}_p \in \mathbb{R}^{n\times n}$ are

$$U_{ij} = Z_h^{\boldsymbol{\alpha}+\boldsymbol{\beta}+\boldsymbol{e}_i+\boldsymbol{e}_j} - Y^{\boldsymbol{\alpha}+\boldsymbol{\beta}+\boldsymbol{e}_i+\boldsymbol{e}_j}, \quad (X_p)_{ij} = (c(\boldsymbol{x}-\boldsymbol{x}_p))^{\boldsymbol{e}_i+\boldsymbol{e}_j},$$

and $\lambda^{\boldsymbol{U}}_{\min}$ and $\lambda^{\boldsymbol{U}}_{\max}$ are the smallest and largest eigenvalues of $\boldsymbol{U}$.

The stability measure S for explicit Euler time stepping in the anisotropic case is

$$S = \inf_{|\boldsymbol{k}|\in]0,\sqrt{n}\pi]} \left[\frac{-2\alpha_{\min}^{\mathrm{Im}(\boldsymbol{\Omega})}}{\max\left(\alpha_{\min}^{\mathrm{Re}(\boldsymbol{\Omega})^2}, \alpha_{\max}^{\mathrm{Re}(\boldsymbol{\Omega})^2}\right) + \max\left(\alpha_{\min}^{\mathrm{Im}(\boldsymbol{\Omega})^2}, \alpha_{\max}^{\mathrm{Im}(\boldsymbol{\Omega})^2}\right)} \right],$$

$$\alpha^X_{\min} = \lambda^X_{\min} - \frac{\mathrm{tr}(\boldsymbol{X})}{n+2}, \quad \alpha^X_{\max} = \lambda^X_{\max} - \frac{\mathrm{tr}(\boldsymbol{X})}{n+2},$$

where the elements of the matrix $\boldsymbol{\Omega}$ are defined as

$$\Omega_{ij} = c^{4+n} \sum_{p\in\mathcal{N}(\boldsymbol{x})} v_p \left(\exp(\hat{\imath}\boldsymbol{k}\cdot(\boldsymbol{x}_p-\boldsymbol{x}))-1\right) \eta(c(\boldsymbol{x}-\boldsymbol{x}_p)) (\boldsymbol{x}-\boldsymbol{x}_p)^{\boldsymbol{e}_i+\boldsymbol{e}_j}.$$

The viscosity ν in condition (4.4) has to be replaced by $\mathrm{tr}(\boldsymbol{\nu})$ in the anisotropic case. We remark that condition (4.4) is then sufficient for stability, but not necessary.

A.2. A Fishelov diffusion operator. We consider a diffusion operator following the Fishelov scheme [13],

$$Q_h f(\boldsymbol{x}) = \nu \frac{c^5}{h^2} \sum_p f(\boldsymbol{x}_p)\eta(\boldsymbol{x}-\boldsymbol{x}_p),$$

where

$$\eta(\boldsymbol{z}) = \nabla^2 W(\boldsymbol{z}), \quad W(\boldsymbol{z}) = \frac{1}{\pi\sqrt{\pi}} \exp(-c^2 z^2),\ z = |\boldsymbol{z}|.$$

Thus,

$$\eta(\boldsymbol{z}) = \frac{1}{\pi\sqrt{\pi}} \left(4c^2z^2-6\right)\exp(-c^2z^2)$$

for constant isotropic viscosity ν.

A Taylor expansion of f around $\boldsymbol{x}$ enables bounding the overall error $E(\boldsymbol{x})$ as in (4.1) with the accuracy measures

$$A_s = \left[\sum_{|\boldsymbol{\alpha}|=s+2} \frac{c^5}{\pi\sqrt{\pi}\boldsymbol{\alpha}!} \left| \sum_p \left(4c^2|\boldsymbol{x}_p-\boldsymbol{x}|^2-6\right)(\boldsymbol{x}_p-\boldsymbol{x})^{\boldsymbol{\alpha}} \right.\right.$$
$$\left.\left. \times \exp\left(-c^2|\boldsymbol{x}_p-\boldsymbol{x}|^2\right) - Y^{\boldsymbol{\alpha}} \right| \right]^{-1}, \ -2 \le s \le 1,$$

$$A_2 = \left[\sum_{|\boldsymbol{\alpha}|=4} \frac{c^4}{\pi\sqrt{\pi}\boldsymbol{\alpha}!} \sum_p \left| \left(4c^2|\boldsymbol{x}_p-\boldsymbol{x}|^2-6\right)(\boldsymbol{x}_p-\boldsymbol{x})^{\boldsymbol{\alpha}} \exp\left(-c^2|\boldsymbol{x}_p-\boldsymbol{x}|^2\right) \right| \right]^{-1},$$

where $Y^{\boldsymbol{\alpha}} = 1$ if $\boldsymbol{\alpha} = 2\boldsymbol{e}_i$ and $Y^{\boldsymbol{\alpha}} = 0$ else. The stability measure S is obtained by substituting the dispersion relation

$$\omega(\boldsymbol{k}) = \frac{\hat{\imath}c^5}{\pi\sqrt{\pi}} \sum_p e^{\hat{\imath}\boldsymbol{k}\cdot(\boldsymbol{x}_p-\boldsymbol{x})} \left(4c|\boldsymbol{x}_p-\boldsymbol{x}|^2-6\right) \times \exp\left(-c|\boldsymbol{x}_p-\boldsymbol{x}|^2\right)$$

into (3.13).

A.3. The diffusion operator of a resampling method. We derive the accuracy and stability measures for a resampling method [8] with constant viscosity ν. From the evolution equation

$$f(\boldsymbol{x}_q, t+\Delta t) = \sum_p v_p(t) f(\boldsymbol{x}_p, t) \mathcal{G}(\boldsymbol{x}_q - \boldsymbol{x}_p, \nu\Delta t),$$
$$\mathcal{G}(\boldsymbol{z}, \nu\Delta t) = \frac{1}{(4\pi\nu\Delta t)^{3/2}} \exp\left(-\frac{z^2}{4\nu\Delta t}\right),$$

one can construct the equivalent diffusion operator for explicit Euler time stepping as

$$Q_h f(\boldsymbol{x}) = \sum_p v_p(t) f(\boldsymbol{x}_p, t) \frac{\mathcal{G}(\boldsymbol{x} - \boldsymbol{x}_p, \nu\Delta t)}{\Delta t} - \frac{f(\boldsymbol{x}, t)}{\Delta t}. \tag{A.1}$$

Fixing the CFL number $\alpha_{\mathrm{CFL}} = \Delta t\nu/h^2$, the accuracy measures are

$$A_s = \left[\sum_{|\boldsymbol{\alpha}|=s+2} \left| \frac{1}{8\pi\sqrt{\alpha_{\mathrm{CFL}}^5 \pi}\boldsymbol{\alpha}!} \sum_p (\boldsymbol{x}_p - \boldsymbol{x})^{\boldsymbol{\alpha}} \right.\right.$$
$$\left.\left. \times \exp\left(-\frac{1}{4\alpha_{\mathrm{CFL}}} |\boldsymbol{x}_p - \boldsymbol{x}|^2\right) - Y^{\boldsymbol{\alpha}} \right| \right]^{-1}, \ -2 \le s \le 1,$$

$$A_2 = 8\pi\sqrt{\alpha_{\mathrm{CFL}}^5 \pi} \left[\sum_{|\boldsymbol{\alpha}|=4} \frac{1}{\boldsymbol{\alpha}!} \sum_p \left| (\boldsymbol{x}_p - \boldsymbol{x})^{\boldsymbol{\alpha}} \times \exp\left(-\frac{1}{4\alpha_{\mathrm{CFL}}} |\boldsymbol{x}_p - \boldsymbol{x}|^2\right) \right| \right]^{-1}, \tag{A.2}$$

where $Y^{\boldsymbol{\alpha}} = 1$ if $\boldsymbol{\alpha} = \mathbf{0}$ or $\boldsymbol{\alpha} = 2\boldsymbol{e}_i$ and $Y^{\boldsymbol{\alpha}} = 0$ else. The stability measure S cannot be given in closed form, but should be defined as the maximum CFL number α_{CFL} such that

$$\left| \sum_p \frac{\exp\left(\hat{\imath}\boldsymbol{k} \cdot (\boldsymbol{x}_p - \boldsymbol{x}) - \frac{1}{4\alpha_{\mathrm{CFL}}} |\boldsymbol{x}_p - \boldsymbol{x}|^2\right)}{\sqrt{4\pi\alpha_{\mathrm{CFL}}}^3} \right| < 1 \ \forall\, |\boldsymbol{k}| \in]0, \sqrt{n}\pi]. \tag{A.3}$$

Numerical exploration of (A.3) reveals that there is a *lower* bound, rather than an upper bound, on the CFL number. The left panel of Figure A.1 shows the dependence of the numerical amplification on the CFL number for uniform Cartesian particle distributions and $r_c/h = 6$. The dashed line marks the CFL number where the amplification is unity. The CFL number hence has to be chosen larger than this minimum value $(\alpha_{\mathrm{CFL}})_{\min}$ in order for the operator to be stable. The minimum value $(\alpha_{\mathrm{CFL}})_{\min}$ depends on the cutoff radius. This dependence is shown in the right panel of Figure A.1. Note that in this method the highest amplifications occur for the smallest wavenumbers. This is because the amplification is simply defined by the numerical quadrature of the heat kernel $\mathcal{G}$ using the rectangular rule. Hence, it is an artifact of the discretization error of the resampling method.

As we do not find an upper bound for the CFL number, a stability measure as it exists for the other diffusion operators cannot be defined for the resampling method. Instabilities in this method thus occur for *small* time steps, and not for large ones.

A.4. A robust diffusion operator in smoothed particle hydrodynamics. Cleary and Monaghan [4] introduced the robust (against particle disorder and jumps

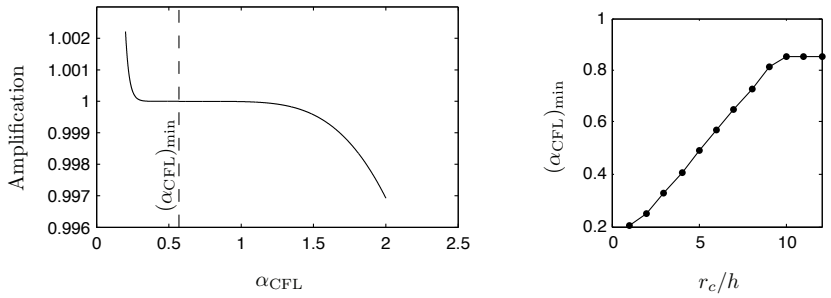

FIG. A.1. *Numerical stability of the resampling method. Left panel: Amplification vs. CFL number α_{CFL} for $r_c/h = 6$. The dashed line marks the CFL number $(\alpha_{CFL})_{min}$ where the amplification is unity. Right panel: Dependence of the minimum CFL number on the cutoff radius.*

in the viscosity) diffusion operator for smoothed particle hydrodynamics (SPH),

$$Q_h f(\boldsymbol{x}) = \sum_p \frac{m_p}{\rho_p}(f(\boldsymbol{x}_p) - f(\boldsymbol{x}))\mu(\boldsymbol{x}, \boldsymbol{x}_p)\eta_\varepsilon(\boldsymbol{x} - \boldsymbol{x}_p), \tag{A.4}$$

where the ratio of mass m_p and density ρ_p can be replaced by the particle volume v_p,

$$\mu(\boldsymbol{x}, \boldsymbol{x}_p) = \frac{4\nu(\boldsymbol{x})\nu(\boldsymbol{x}_p)}{\nu(\boldsymbol{x}) + \nu(\boldsymbol{x}_p)} \quad \text{and} \quad \eta_\varepsilon(\boldsymbol{z}) = \frac{2}{\pi\sqrt{\pi}\varepsilon^5}\exp\left(-\frac{|\boldsymbol{z}|^2}{\varepsilon^2}\right) = \frac{1}{\varepsilon^5}\eta(\boldsymbol{z}\varepsilon)\,.$$

Due to the nonlinear mean $\mu(\boldsymbol{x}, \boldsymbol{x}_p)$, we did not find a bound for the overall error of the form given in (4.2). However, using the multivariate version of Faà di Bruno's formula [5, 17], one can evaluate $D^{\boldsymbol{\beta}}\mu(\boldsymbol{x}, \boldsymbol{x})$, where the derivative is applied with respect to the second argument, as

$$\begin{aligned} D^{\boldsymbol{\beta}}\mu(\boldsymbol{x}, \boldsymbol{y}) &= \frac{\partial^{|\boldsymbol{\beta}|}}{\partial^{\beta_1} y_1 \dots \partial^{\beta_n} y_n}\mu(\boldsymbol{x}, \boldsymbol{y}) \\ &= \sum_{1 \le \lambda \le |\boldsymbol{\beta}|} \mu_\nu^{(\lambda)}(\nu_p) \sum_{s=1}^{\lambda} \sum_{p_s(\boldsymbol{\beta}, \lambda)} (\boldsymbol{\beta}!) \prod_{j=1}^{s} \frac{[D^{\boldsymbol{l}_j}\nu_p]^{k_j}}{(k_j!)[\boldsymbol{l}_j!]^{k_j}}, \end{aligned} \tag{A.5}$$

where $\mu_\nu(\nu_p) = \frac{4\nu\nu_p}{\nu+\nu_p}$, $\nu = \nu(\boldsymbol{x})$, $\nu_p = \nu(\boldsymbol{y})$, $\boldsymbol{l}_i \in \mathbb{N}^n$,

$$\begin{aligned} p_s(\boldsymbol{\beta}, \lambda) = \Big\{ &(k_1, \dots, k_s; \boldsymbol{l}_1, \dots, \boldsymbol{l}_s) : k_i > 0, \\ &\boldsymbol{0} \prec \boldsymbol{l}_1 \prec \dots \prec \boldsymbol{l}_s, \sum_{i=1}^{s} k_i = \lambda \text{ and } \sum_{i=1}^{s} k_i \boldsymbol{l}_i = \boldsymbol{\beta} \Big\}. \end{aligned}$$

For $\boldsymbol{a}, \boldsymbol{b} \in \mathbb{N}^n$, $\boldsymbol{a} \prec \boldsymbol{b}$ means that one of the following holds:

1. $|\boldsymbol{a}| < |\boldsymbol{b}|$,
2. $|\boldsymbol{a}| = |\boldsymbol{b}|$ and $a_1 < b_1$, or
3. $|\boldsymbol{a}| = |\boldsymbol{b}|$, $a_1 = b_1, \dots, a_k = b_k$ and $a_{k+1} < b_{k+1}$ for some k, $1 \le k \le n$.

In other words, the vectors $\boldsymbol{l}_i$ are the partitions of $\boldsymbol{\beta}$, the scalars k_i their multiplicities. The variable λ counts the number of partitions, while the variable s counts the number of different partitions. For example,

$$\boldsymbol{\beta} = \underbrace{(3,0,0)}_{\substack{\boldsymbol{l}_1=(3,0,0), s=1, \\ \lambda=1, k_1=1}} = \underbrace{(2,0,0) + (1,0,0)}_{\substack{\boldsymbol{l}_1=(1,0,0), \boldsymbol{l}_2=(2,0,0), \\ s=2, \lambda=2, k_1=1, k_2=1}} = \underbrace{(1,0,0) + (1,0,0) + (1,0,0)}_{\substack{\boldsymbol{l}_1=(1,0,0), s=1, \\ \lambda=3, k_1=3}}.$$

Note that $p_s(\boldsymbol{\beta}, \lambda)$ may be empty.

Expressing the λth derivative $\mu_\nu^{(\lambda)}$ in terms of ν and substituting in (A.5) yields the closed-form expression for the partial derivatives of μ:

$$D^{\boldsymbol{\beta}}\mu(\boldsymbol{x}, \boldsymbol{y}) = \sum_{1 \le \lambda \le |\boldsymbol{\beta}|} \frac{4(-1)^{\lambda+1}(\lambda!)\nu(\boldsymbol{x})^2}{(\nu(\boldsymbol{x}) + \nu(\boldsymbol{y}))^{\lambda+1}} \sum_{s=1}^{\lambda} \sum_{p_s(\boldsymbol{\beta},\lambda)} (\boldsymbol{\beta}!) \prod_{j=1}^{s} \frac{[D^{\boldsymbol{l}_j}\nu(\boldsymbol{y})]^{k_j}}{(k_j!)[\boldsymbol{l}_j!]^{k_j}}$$

for $|\boldsymbol{\beta}| > 0$. Taylor-expanding $\mu(\boldsymbol{x}, \boldsymbol{x}_p)$ around $\boldsymbol{x}$ and computing the remainder term according to Taylor's theorem, we can thus write

$$\mu(\boldsymbol{x}, \boldsymbol{x}_p) = \sum_{|\boldsymbol{\beta}|=0}^{n} \frac{(\boldsymbol{x}_p - \boldsymbol{x})^{\boldsymbol{\beta}}}{\boldsymbol{\beta}!} D^{\boldsymbol{\beta}}\mu(\boldsymbol{x}, \boldsymbol{x}) + \sum_{|\boldsymbol{\beta}|=n+1} \frac{(\boldsymbol{x}_p - \boldsymbol{x})^{\boldsymbol{\beta}}}{\boldsymbol{\beta}!} R^{\mu}_{\boldsymbol{\beta}}(\boldsymbol{x}_p),$$

where

$$R^{\nu}_{\boldsymbol{\beta}}(\boldsymbol{x}_p) = |\boldsymbol{\beta}| \int_0^1 (1-t)^{|\boldsymbol{\beta}|-1} D^{\boldsymbol{\beta}}\mu(\boldsymbol{x}, \boldsymbol{x} + t(\boldsymbol{x}_p - \boldsymbol{x}))\mathrm{d}t.$$

This means that

$$\begin{aligned}
E(\boldsymbol{x}) = \Bigg| & \sum_{|\boldsymbol{\alpha}|=1}^{r+1} \sum_{|\boldsymbol{\beta}|=0}^{r+1-|\boldsymbol{\alpha}|} D^{\boldsymbol{\alpha}} f(\boldsymbol{x}) D^{\boldsymbol{\beta}}\mu(\boldsymbol{x}, \boldsymbol{x}) \\
& \times \left[\frac{1}{\boldsymbol{\alpha}!\boldsymbol{\beta}!} \sum_p v_p (\boldsymbol{x}_p - \boldsymbol{x})^{\boldsymbol{\alpha}+\boldsymbol{\beta}} \eta_\varepsilon(\boldsymbol{x} - \boldsymbol{x}_p) - Y^{\boldsymbol{\alpha}+\boldsymbol{\beta}} \right] \\
& + \sum_{|\boldsymbol{\alpha}|=1}^{r+1} \sum_{|\boldsymbol{\beta}|=r+2-|\boldsymbol{\alpha}|} D^{\boldsymbol{\alpha}} f(\boldsymbol{x}) \\
& \times \frac{1}{\boldsymbol{\alpha}!\boldsymbol{\beta}!} \sum_p v_p R^{\mu}_{\boldsymbol{\beta}}(\boldsymbol{x}_p)(\boldsymbol{x}_p - \boldsymbol{x})^{\boldsymbol{\alpha}+\boldsymbol{\beta}} \eta_\varepsilon(\boldsymbol{x} - \boldsymbol{x}_p) \\
& + \sum_{|\boldsymbol{\alpha}|=r+2} \frac{1}{\boldsymbol{\alpha}!} \sum_p v_p R^{f}_{\boldsymbol{\alpha}}(\boldsymbol{x}_p)\mu(\boldsymbol{x}, \boldsymbol{x}_p)(\boldsymbol{x}_p - \boldsymbol{x})^{\boldsymbol{\alpha}} \eta_\varepsilon(\boldsymbol{x} - \boldsymbol{x}_p) \Bigg| \\
\le & \sum_{s=-1}^{0} \varepsilon^s \|f\|_{W^{s+2,\infty}(B_{r_c}[\boldsymbol{x}_p])} \|\nu\|_{W^{s+1,\infty}(B_{r_c}[\boldsymbol{x}_p])} \sum_{|\boldsymbol{\alpha}|=1}^{s+2} \sum_{|\boldsymbol{\beta}|=s+2-|\boldsymbol{\alpha}|} \\
& \times \left| \frac{\varepsilon^2}{\boldsymbol{\alpha}!\boldsymbol{\beta}!} \sum_p v_p \left(\frac{\boldsymbol{x}_p - \boldsymbol{x}}{\varepsilon} \right)^{\boldsymbol{\alpha}+\boldsymbol{\beta}} \eta_\varepsilon(\boldsymbol{x} - \boldsymbol{x}_p) - Y^{\boldsymbol{\alpha}+\boldsymbol{\beta}} \right| \\
& + \sum_{s=1}^{r-1} \varepsilon^s \|f\|_{W^{s+2,\infty}(B_{r_c}[\boldsymbol{x}_p])} \|\mu\|_{W^{s+1,\infty}(B_{r_c}[\boldsymbol{x}_p])} \sum_{|\boldsymbol{\alpha}|=1}^{s+2} \sum_{|\boldsymbol{\beta}|=s+2-|\boldsymbol{\alpha}|} \\
& \times \left| \frac{\varepsilon^2}{\boldsymbol{\alpha}!\boldsymbol{\beta}!} \sum_p v_p \left(\frac{\boldsymbol{x}_p - \boldsymbol{x}}{\varepsilon} \right)^{\boldsymbol{\alpha}+\boldsymbol{\beta}} \eta_\varepsilon(\boldsymbol{x} - \boldsymbol{x}_p) \right|
\end{aligned}$$

$$+\varepsilon^r \|f\|_{W^{r+2,\infty}(B_{r_c}[\boldsymbol{x}_p])} \|\mu\|_{W^{r+1,\infty}(B_{r_c}[\boldsymbol{x}_p])} \sum_{|\boldsymbol{\alpha}|=1}^{r+2} \sum_{|\boldsymbol{\beta}|=r+2-|\boldsymbol{\alpha}|}$$

$$\times \frac{\varepsilon^2}{\boldsymbol{\alpha}!\boldsymbol{\beta}!} \sum_p \left| v_p \left(\frac{\boldsymbol{x}_p - \boldsymbol{x}}{\varepsilon} \right)^{\boldsymbol{\alpha}+\boldsymbol{\beta}} \eta_\varepsilon(\boldsymbol{x} - \boldsymbol{x}_p) \right|, \tag{A.6}$$

where $R^f_{\boldsymbol{\alpha}}(\boldsymbol{x}_p) = |\boldsymbol{\alpha}| \int_0^1 (1-t)^{|\boldsymbol{\alpha}|-1} D^{\boldsymbol{\alpha}} f(\boldsymbol{x} + t(\boldsymbol{x}_p - \boldsymbol{x}))\mathrm{d}t$, $Y^{\boldsymbol{\gamma}} = 1$ if $\boldsymbol{\gamma} = 2\boldsymbol{e}_i$, and $Y^{\boldsymbol{\gamma}} = 0$ else. We are thus able to define an upper bound on the overall error $E(\boldsymbol{x})$ as

$$E(\boldsymbol{x}) \leq \sum_{s=-2}^{0} \frac{h^s}{A_s(\boldsymbol{x})} \|f\|_{W^{s+2,\infty}(B_{r_c}[\boldsymbol{x}])} \|\nu\|_{W^{s+1,\infty}(B_{r_c}[\boldsymbol{x}])}$$

$$+ \sum_{s=1}^{2} \frac{h^s}{A^*_s(\boldsymbol{x})} \|f\|_{W^{s+2,\infty}(B_{r_c}[\boldsymbol{x}])} \|\mu\|_{W^{s+1,\infty}(B_{r_c}[\boldsymbol{x}])},$$

where

$$A_s(\boldsymbol{x}) = \infty,\ s = -2,$$

$$A_s(\boldsymbol{x}) = \left[\sum_{|\boldsymbol{\alpha}|=1}^{s+2} \sum_{|\boldsymbol{\beta}|=s+2-|\boldsymbol{\alpha}|} \frac{1}{\boldsymbol{\alpha}!\boldsymbol{\beta}!} \times \left| \sum_p v_p c^{s+5} (\boldsymbol{x}_p - \boldsymbol{x})^{\boldsymbol{\alpha}+\boldsymbol{\beta}} \eta(c(\boldsymbol{x} - \boldsymbol{x}_p)) - Y^{\boldsymbol{\alpha}+\boldsymbol{\beta}} \right| \right]^{-1},\ -1 \leq s \leq 1,$$

$$A^*_s(\boldsymbol{x}) = \left[\sum_{|\boldsymbol{\alpha}|=1}^{4} \sum_{|\boldsymbol{\beta}|=4-|\boldsymbol{\alpha}|} \frac{1}{\boldsymbol{\alpha}!\boldsymbol{\beta}!} \times \sum_p \left| v_p c^7 (\boldsymbol{x}_p - \boldsymbol{x})^{\boldsymbol{\alpha}+\boldsymbol{\beta}} \eta(c(\boldsymbol{x} - \boldsymbol{x}_p)) \right| \right]^{-1},\ s = 2.$$

The stability measure S is obtained by substituting the dispersion relation

$$\omega(\boldsymbol{k}) = 2\hat{\imath}c^5 \sum_p v_p \left[\exp\left(\hat{\imath}\boldsymbol{k} \cdot (\boldsymbol{x}_p - \boldsymbol{x})\right) - 1 \right] \eta(c(\boldsymbol{x} - \boldsymbol{x}_p))$$

into (3.13).

Appendix B. A three-dimensional advection-diffusion test case. The test case considered in this paper consists of solving the advection-diffusion equation

$$\frac{\partial f}{\partial t} + \nabla \cdot (f\boldsymbol{u}) = \nabla \cdot (\nu \nabla f) \quad \text{in } \mathbb{R}^3 \times [0, T]$$

with the velocity field, the viscosity field, and the initial concentration given by

$$\boldsymbol{u}(\boldsymbol{x}) = [\cos x \sin y \sin z,\ \sin x \cos y \sin z,\ \sin x \sin y \cos z]^{\mathrm{T}},$$
$$\nu(\boldsymbol{x}) = \sin x \sin y \sin z + 1,\ \text{and}$$
$$f_0(\boldsymbol{x}) = f(\boldsymbol{x}, t = 0) \ = \ \sin x \sin y \sin z,$$

respectively. The analytical solution of this problem is

$$f(\boldsymbol{x}, t) = \sin x \sin y \sin z \exp(-3t).$$

The problem is numerically computed in a cube of edge length $L = 2\pi$ with periodic boundary conditions, and thus no boundary effects affect the numerical solution. Explicit Euler time stepping is used for time integration, hence

$$\begin{aligned} f_p(t+\Delta t) &= \frac{v_p(t)}{v_p(t+\Delta t)}[f_p(t) + \Delta t Q_h f_p(t)], \\ \boldsymbol{x}_p(t+\Delta t) &= \boldsymbol{x}_p(t) + \Delta t \boldsymbol{u}(\boldsymbol{x}_p(t)), \\ v_p(t+\Delta t) &= v_p(t)[1 + \Delta t \nabla \cdot \boldsymbol{u}(\boldsymbol{x}_p(t))], \end{aligned}$$

where the subscript p indicates properties of particle p. For remeshing, the concentration field f is interpolated from the particle positions $\boldsymbol{x}_p$ to the positions $\tilde{\boldsymbol{x}}_p$ of the nodes of a uniform Cartesian mesh using the third-order accurate M_4' interpolation kernel, introduced as the W_4 function by Monaghan [24]:

$$M_4'(z) = \begin{cases} 0, & |z| > 2, \\ \frac{1}{2}(2-|z|)^2(1-|z|), & 1 \le |z| \le 2, \\ 1 - \frac{5}{2}z^2 + \frac{3}{2}|z|^3, & |z| \le 1\,, \end{cases} \tag{B.1}$$

where $z = (\tilde{x}_p - x_p)/h$ and h is the mesh spacing of the regular Cartesian particle distribution $\tilde{\boldsymbol{x}}_p$. The concentration field after remeshing hence becomes

$$\tilde{f}_p(t) = \frac{1}{h^3} \sum_q v_q(t) f_q(t) \prod_{i=1}^{3} M_4' \left[\frac{(\tilde{\boldsymbol{x}}_p - \boldsymbol{x}_q(t))_i}{h} \right].$$

Acknowledgment. We thank Christian L. Müller (MOSAIC Group, ETH Zurich) for many useful discussions.

REFERENCES

[1] T. Belytschko, Y. Krongauz, D. Organ, M. Fleming, and P. Krysl, *Meshless methods: An overview and recent developments*, Comput. Method. Appl. Mech. Engrg., 139 (1996), pp. 3–47.

[2] J. P. Choquin and B. Lucquin-Desreux, *Accuracy of a deterministic particle method for Navier-Stokes equations*, Internat. J. Numer. Methods Fluids, 8 (1988), pp. 1439–1458.

[3] A. J. Chorin, *Numerical study of slightly viscous flow*, J. Fluid Mech., 57 (1973), pp. 785–796.

[4] P. W. Cleary and J. J. Monaghan, *Conduction modelling using smoothed particle hydrodynamics*, J. Comput. Phys., 148 (1999), pp. 227–264.

[5] G. M. Constantine and T. H. Savits, *A multivariate Faà di Bruno formula with applications*, Trans. Amer. Math. Soc., 348 (1996), pp. 503–520.

[6] G.-H. Cottet and P. Koumoutsakos, *Vortex Methods: Theory and Practice*, Cambridge University Press, New York, 2000.

[7] G.-H. Cottet and S. Mas-Gallic, *Une méthode de décomposition pour une équation de type convection-diffusion combinant résolution explicite et méthode particulaire (a splitting algorithm for a convection-diffusion equation based on combining a particle method with an explicit solution)*, C. R. Acad. Sci. Paris Sér. I Math., 297 (1983), pp. 133–136.

[8] G. H. Cottet and S. Mas-Gallic, *A particle method to solve the Navier-Stokes system*, Numer. Math., 57 (1990), pp. 805–827.

[9] P. Degond and S. Mas-Gallic, *The weighted particle method for convection-diffusion equations. Part* 1: *The case of an isotropic viscosity*, Math. Comp., 53 (1989), pp. 485–507.

[10] P. Degond and S. Mas-Gallic, *The weighted particle method for convection-diffusion equations. Part* 2: *The anisotropic case*, Math. Comp., 53 (1989), pp. 509–525.

[11] P. Degond and F.-J. Mustieles, *A deterministic approximation of diffusion equations using particles*, SIAM J. Sci. Statist. Comput., 11 (1990), pp. 293–310.

[12] J. D. Eldredge, A. Leonard, and T. Colonius, *A general deterministic treatment of derivatives in particle methods*, J. Comput. Phys., 180 (2002), pp. 686–709.

[13] D. Fishelov, *A new vortex scheme for viscous flows*, J. Comput. Phys., 86 (1990), pp. 211–224.
[14] T.-P. Fries and H.-G. Matthies, *Classification and Overview of Meshfree Methods*, Informatikbericht 2003-03, Technical University Braunschweig, 2004.
[15] A. Gharakhani, *A Higher Order Vorticity Redistribution Method for 3-D Diffusion in Free Space*, Technical report, Sandia National Laboratories, 2000.
[16] R. Gruber and V. Keller, *HPC@GreenIT*, Springer, New York, 2010.
[17] M. Hardy, *Combinatorics of partial derivatives*, Electron. J. Combin., 13 (2006), pp. 1–13.
[18] P. Koumoutsakos, *Multiscale flow simulations using particles*, Annu. Rev. Fluid Mech., 37 (2005), pp. 457–487.
[19] P. Lancaster and K. Salkauskas, *Surfaces generated by moving least squares methods*, Math. Comp., 37 (1981), pp. 141–158.
[20] W. K. Liu, Y. Chen, R. Aziz Uras, and C. T. Chang, *Generalized multiple scale reproducing kernel particle methods*, Comput. Methods Appl. Mech. Engrg., 139 (1996), pp. 91–157.
[21] W. K. Liu, S. Jun, and Y. F. Zhang, *Reproducing kernel particle methods*, Internat. J. Numer. Methods Fluids, 20 (1995), pp. 1081–1106.
[22] S. Mas-Gallic, *Contribution à l'Analyse Numérique des Méthodes Particulaires*, Ph.D. thesis, Université de Pierre et Marie Curie, Paris, 1987.
[23] V. Maz'ya and G. Schmidt, *Approximate Approximations*, Math. Surveys Monogr. 141, AMS, Providence, RI, 2007.
[24] J. J. Monaghan, *Extrapolating B splines for interpolation*, J. Comput. Phys., 60 (1985), pp. 253–262.
[25] J. J. Monaghan, *Smoothed particle hydrodynamics*, Rep. Progr. Phys., 68 (2005), pp. 1703–1759.
[26] M. Perlmann, *On the accuracy of vortex methods*, J. Comput. Phys., 59 (1985), pp. 200–223.
[27] P. A. Raviart, *An analysis of particle methods*, in Numerical Methods in Fluid Dynamics, F. Brezzi, ed., Lecture Notes in Math. 1127, Springer, Berlin, 1985, pp. 244–323.
[28] G. Russo, *A Lagrangian vortex method for the incompressible Navier-Stokes equations*, in Vortex Dynamics and Vortex Methods, C. R. Anderson and C. Greengard, eds., Lectures in Appl. Math. 28, AMS, Providence, RI, 1991, pp. 585–596.
[29] G. Russo, *A deterministic vortex method for the Navier-Stokes equations*, J. Comput. Phys., 108 (1993), pp. 84–94.
[30] I. F. Sbalzarini, J. H. Walther, M. Bergdorf, S. E. Hieber, E. M. Kotsalis, and P. Koumoutsakos, *PPM—a highly efficient parallel particle-mesh library for the simulation of continuum systems*, J. Comput. Phys., 215 (2006), pp. 566–588.
[31] B. Schrader, S. Reboux, and I. F. Sbalzarini, *Discretization correction of general integral PSE operators in particle methods*, J. Comput. Phys., 229 (2010), pp. 4159–4182.
[32] S. Shankar and L. van Dommelen, *A new diffusion procedure for vortex methods*, J. Comput. Phys., 127 (1996), pp. 88–109.
[33] L. Verlet, *Computer experiments on classical fluids.* I. *Thermodynamical properties of Lennard-Jones molecules*, Phys. Rev., 159 (1967), pp. 98–103.
[34] S. Williams, A. Waterman, and D. Patterson, *Roofline: An insightful visual performance model for multicore architectures*, Comm. ACM, 52 (2009), pp. 65–76.